

Radiofrequency spectroscopy of one-dimensional trapped Bose polarons: crossover from the adiabatic to the diabatic regime

S. I. Mistakidis,^{1,2} G.M. Koutentakis,^{1,3} F. Grusdt,^{4,5} H. R. Sadeghpour,² and P. Schmelcher^{1,3}

¹*Center for Optical Quantum Technologies, Department of Physics, University of Hamburg, Luruper Chaussee 149, 22761 Hamburg Germany*

²*ITAMP, Center for Astrophysics | Harvard & Smithsonian, Cambridge, MA 02138 USA*

³*The Hamburg Centre for Ultrafast Imaging, University of Hamburg, Luruper Chaussee 149, 22761 Hamburg, Germany*

⁴*Department of Physics and Arnold Sommerfeld Center for Theoretical Physics (ASC), Ludwig-Maximilians-Universität München, Theresienstr. 37, München D-80333, Germany*

⁵*Munich Center for Quantum Science and Technology (MCQST), Schellingstr. 4, D-80799 München, Germany*

(Dated: May 4, 2021)

We investigate the crossover of the impurity-induced dynamics, in trapped one-dimensional Bose polarons subject to radio frequency (rf) pulses of varying intensity, from an adiabatic to a diabatic regime. Utilizing adiabatic pulses for either weak repulsive or attractive impurity-medium interactions, a multitude of polaronic excitations or mode-couplings of the impurity-bath interaction with the collective breathing motion of the bosonic medium are spectrally resolved. We find that for strongly repulsive impurity-bath interactions, a temporal orthogonality catastrophe manifests in resonances in the excitation spectra where impurity coherence vanishes. When two impurities are introduced, impurity-impurity correlations, for either attractive or strong repulsive couplings, induce a spectral shift of the resonances with respect to the single impurity. For a heavy impurity, the polaronic peak is accompanied by a series of equidistant side-band resonances, related to interference of the impurity spin dynamics and the sound waves of the bath. In all cases, we enter the diabatic transfer regime for an increasing bare Rabi frequency of the rf field with a Lorentzian spectral shape featuring a single polaronic resonance. The findings in this work on the effects of external trap, rf pulse and impurity-impurity interaction should have implications for the new generations of cold-atom experiments.

I. INTRODUCTION

The concept of quasiparticles [1, 2] such as polarons [3, 4], mobile impurities dressed by their many-body (MB) host has found considerable interest in the cold-atom community, due to the precise tunability of inter-atomic interactions with tools such as Fano-Feshbach resonances [5, 6]. Spectroscopic techniques, such as rf and Ramsey spectroscopy [7–11] permit the characterization of quasiparticle states. Utilizing these probes and depending on the quantum statistics of the host both Bose [12–16] and Fermi [7, 8, 17] polarons have been recently realized mainly in multidimensional settings. The one-dimensional (1D) Bose and Fermi polarons are less explored [18–20].

The above experimental findings have been corroborated by theory [21, 22], e.g. using variational approaches [23–27] and renormalization group methods [28, 29]. These methods initially aimed to address the equilibrium polaron properties, such as their effective mass [23, 30, 31], induced interactions [24, 32], bound bipolaron [3, 4, 33] and trimeron [34] states. More recently, the nonequilibrium dynamics of polarons [25, 26, 29, 35–39] have attempted to address issues, such as the collisional properties with the host bath particles [18, 40–45], tunneling in optical lattices [46–49], dynamics of doped insulators [50–52], induced correlations [53, 54], relaxation processes [37, 55] and dynamical decay, i.e. the temporal orthogonality catastrophe (TOC) [25, 53, 56].

Here, we probe the dynamics of Bose polarons in 1D, where correlations can be enhanced, with the rf spectroscopy. The rf spectroscopy provides a powerful and well-established experimental toolkit [9, 14, 15, 57] for monitoring the polaronic states and the correlation dynamics. Recall that within a typical rf spectroscopy protocol, the MB system is prepared in its equilibrium state and subsequently a specific pulse drives the impurity atoms from their non-interacting to the interacting with the host spin state (injection spectroscopy) or vice versa (ejection spectroscopy) [58–60].

The rf scheme thus enables us to probe the polaron excitation at different response regimes of the impurities spin-flip dynamics, compared to the characteristic timescale of their atomic motion. It should be emphasized that irrespectively of the spatial dimension the crossover of the dynamical response of Bose polarons from weak to strong Rabi coupling of the involved spin states has not been systematically studied. Therefore, it would be particularly interesting to unravel the dependence of the polaron states and their correlation properties with respect to the intensity of the rf pulse, a study that can potentially lead to controlling the polaron states. For instance, in the extreme limit of an intense rf field, the spin-transfer is much faster (diabatic) than the characteristic timescale of the atomic motion related to phononic emission. Then, we would expect that the spatial and spin degrees-of-freedom are decoupled and thus correlation is negligible. In contrast, weaker pulses lead

to a slower (adiabatic) transfer when compared to the timescale set by the external confinement. As such, it is possible to retrieve information regarding the energy content of the system in terms of its eigenstates.

A prototype system consists of one or two spinor impurity bosons embedded in a 1D harmonically trapped Bose-Einstein condensate (BEC). To monitor the excitation dynamics of this setting when subjected to an injection rf pulse, we deploy the variational nonperturbative method Multi-Layer Multi-Configuration Time-Dependent Hartree method for atomic mixtures (ML-MCTDHX) [61–63], which enables us to capture the interparticle correlations.

The formation of attractive or repulsive Bose polarons is considered for weakly attractive or repulsive impurity-medium coupling. More precisely, for pulses with a bare Rabi frequency smaller or equal to the phononic excitation frequency, a variety of polaronic resonances appear, reflecting the mode-coupling of the impurity motion to the collective breathing of the bosonic bath [64]. The motionally excited polaronic states exhibit a decreasing quasi-particle residue. Remarkably, for strongly repulsive impurity-bath interactions, TOC of the Bose polaron [25, 53, 56], manifests in the spectrum which saturates for long pulse times. Here, the spectral response experiences a multitude of resonances corresponding to distinct superpositions of lower-lying energy states of the impurity. The rate of the polaron decay via TOC is found to be inherently faster for increasing bath-impurity spatial overlap, a process that can be controlled with detuning of the rf field. The suppressed coherence of the impurity in the course of the TOC means that the polaron also vanishes.

In the case of a heavy impurity, irrespective of the impurity-medium interaction and the bare Rabi frequency (except the diabatic case), a polaronic resonance is always present, accompanied by a series of equidistant side peaks and troughs. This latter structure originates from the interference of the sound waves of the background with the impurity spin dynamics. Moreover regardless of the impurity-medium coupling and mass ratio, increasing the bare Rabi frequency (larger than the characteristic trap frequency), allows us to systematically probe the diabatic spin-transfer regime with the spectrum featuring a Lorentzian shape with a single polaronic resonance.

For two non-interacting bosonic impurities and for either attractive or strong repulsive impurity-medium couplings, a small shift of the spectral resonance, compared with the single impurity case is observed. This fact elucidates the presence of induced impurity-impurity correlations mediated by the BEC medium [53, 54, 56]. In all cases, the resonance position can be tuned by varying the impurity-bath coupling or the bare Rabi frequency.

This work is organized as follows. Section II introduces the setup under consideration and the employed rf protocol to induce the impurity nonequilibrium dynamics. Additionally, the different theoretical approaches used for

the interpretation of the impurity rf spectrum are outlined. In Sec. III we analyze in detail the resultant spectral response for different impurity-medium interactions and importantly address the crossover from adiabatic to diabatic spin dynamics for different intensities of the rf pulse. The two-body processes contributing to the spectrum of two non-interacting impurities are discussed in Sec. IV. The emergent spectral response of an impurity heavier than the atoms of the corresponding medium for different impurity-BEC coupling and rf intensities is presented in Sec. V. We summarize and provide perspectives for future endeavors in Section VI. Appendix A elaborates on the details of the diabatic approximation.

II. SPECTROSCOPY SCHEME AND METHODOLOGICAL APPROACHES

A. Hamiltonian and radiofrequency protocol

To emulate the rf injection spectroscopy scheme [9, 14, 15, 24, 38], we consider a highly particle imbalanced multicomponent bosonic system. It consists of $N_I = 1, 2$ non-interacting bosonic impurities (I) possessing a $1/2$ pseudospin [65], immersed in a structureless bosonic medium (B) with $N_B = 100$ atoms. The impurity-bath system here is mass balanced, $m_B = m_I$ (unless stated otherwise), while the involved components are harmonically confined in the same 1D external potential of frequency ω . This scenario can be realized, for instance, by assuming a ^{87}Rb gas. Here, the impurity pseudospin degree of freedom corresponds e.g. to the hyperfine states $|\uparrow\rangle \equiv |F = 1, m_F = 1\rangle$ and $|\downarrow\rangle \equiv |F = 1, m_F = -1\rangle$ whilst the bath bosons are in the $|F = 2, m_F = 1\rangle$ state [66–68]. Another experimentally relevant setting is, to a good approximation, a mixture of isotopes containing two hyperfine states of ^{85}Rb for the impurity subsystem and of ^{87}Rb for the bosonic bath.

The resulting MB Hamiltonian reads

$$\hat{H} = \hat{H}_B^0 + \hat{H}_{BB} + \sum_{a=\uparrow,\downarrow} \hat{H}_a^0 + \hat{H}_{BI} + \hat{H}_S. \quad (1)$$

Here, $\hat{H}_B^0 = \int dx \hat{\Psi}_B^\dagger(x) \left(-\frac{\hbar^2}{2m_B} \frac{d^2}{dx^2} + \frac{1}{2} m_B \omega^2 x^2 \right) \hat{\Psi}_B(x)$, and $\hat{H}_a^0 = \int dx \hat{\Psi}_a^\dagger(x) \left(-\frac{\hbar^2}{2m_I} \frac{d^2}{dx^2} + \frac{1}{2} m_I \omega^2 x^2 \right) \hat{\Psi}_a(x)$ denote the non-interacting Hamiltonian of the BEC and the impurity respectively. The field operator $\hat{\Psi}_B(x)$ refers to the BEC while $\hat{\Psi}_a(x)$ to the spin- a impurity atoms with $a = \{\uparrow, \downarrow\}$. We further consider that the dominant interparticle interaction is an s -wave one since we operate in the ultracold regime [69]. As such both intra- (g_{BB}) and inter-component (g_{BI}) interactions are adequately described by contact ones. Moreover, $\hat{H}_{BB} = (g_{BB}/2) \int dx \hat{\Psi}_B^\dagger(x) \hat{\Psi}_B^\dagger(x) \hat{\Psi}_B(x) \hat{\Psi}_B(x)$ corresponds to the contact intracomponent interaction term of the bosonic bath. Also, in order to mimic the rf scheme only the spin- \uparrow component of the impurities

couples with the BEC and thus $g_{B\uparrow} \equiv g_{BI}$, while the spin- \downarrow one is non-interacting namely $g_{B\downarrow} = 0$. Additionally, the relevant intercomponent interaction term reads $\hat{H}_{BI} = g_{BI} \int dx \hat{\Psi}_B^\dagger(x) \hat{\Psi}_\uparrow^\dagger(x) \hat{\Psi}_\uparrow(x) \hat{\Psi}_B(x)$.

It is worth mentioning that the three-dimensional s -wave scattering length, $a_{\sigma\sigma'}^s$, for intra- or inter-species interactions, $\sigma = B, \uparrow, \downarrow$ is related to the effective one-dimensional coupling strength [69]. As a consequence $g_{\sigma\sigma'}$, is experimentally tunable either by adjusting $a_{\sigma\sigma'}^s$ using Feshbach resonances [5, 6] or by means of the transversal confinement frequency ω_\perp with the aid of confinement-induced resonances [69].

The impurity spin Hamiltonian with Rabi coupling is,

$$\hat{H}_S = \frac{\hbar\Omega_{R0}(t)}{2} \hat{S}_x + \frac{\hbar\Delta}{2} \hat{S}_z, \quad (2)$$

with $\Omega_{R0}(t)$ and $\Delta = \nu - \nu_0$ referring to the time-dependent bare Rabi frequency and the detuning of the rf field [9, 14] when the bosonic bath is absent. In particular, $\Omega_{R0}(t)$ and Δ characterize the intensity and frequency respectively of the applied rf pulse [70]. Notice also that the total spin operator is $\hat{S} = \int dx \hat{S}(x) = \int dx \sum_{ab} \hat{\Psi}_a^\dagger(x) \boldsymbol{\sigma}_{ab} \hat{\Psi}_b(x)$, with $\boldsymbol{\sigma}$ denoting the Pauli vector [71].

For convenience, in the following, the MB Hamiltonian of Eq. (1) is rescaled with respect to $\hbar\omega$. Accordingly, the length, time, detuning and interaction strengths are expressed in units of $\alpha = \sqrt{\hbar/(m\omega)}$, ω^{-1} , ω and $\hbar\omega\alpha = \sqrt{(\hbar^3\omega)/m}$ respectively. A corresponding experimental realization of our one-dimensional setup e.g. when considering a ^{87}Rb bosonic gas with $g_{BB} = 0.5\sqrt{\hbar^3\omega/m} \approx 3.55 \times 10^{-38}$ Jm can be easily achieved, for instance, by using a trap frequency $\omega = 2\pi \times 100$ Hz while the transverse frequencies $\omega_\perp \approx 2\pi \times 5.1$ KHz. Here, temperature effects are suppressed for $k_B T \ll \frac{3^{4/3}}{16} (\frac{\alpha_\perp^2 N_B^2}{a_{BB}^2 \alpha})^{2/3} \hbar\omega = 316\hbar\omega \approx 1.5 \mu\text{K}$ [72], where k_B is the Boltzmann constant, T is the temperature of the bosonic environment and $\alpha_\perp = \sqrt{\hbar/(m\omega_\perp)}$ is the transversal confinement length scale.

To trigger the nonequilibrium dynamics, see Fig. 1 (a), we prepare the bosonic bath in its ground state with $g_{BB} = 0.5$ and the impurities in their spin- \downarrow state being non-interacting with the bath. As a result the system is initialized in the $|N_I/2, -N_I/2\rangle = \bigotimes_{i=1}^{N_I} |\downarrow\rangle_i$ spin configuration where $\langle \hat{H}_{BI} \rangle = 0$. The spinor part of the wave function is expressed in the basis of the total spin, namely $|S, S_z\rangle$ [71]. Moreover, the spatial part $|\Psi_{BI}^0\rangle$ of the system's ground state satisfies the eigenvalue equation $(\hat{H} - \hat{H}_{BI}) |\Psi_{BI}^0\rangle |N_I/2, -N_I/2\rangle = E_0 |\Psi_{BI}^0\rangle |N_I/2, -N_I/2\rangle$, with $\hat{H}_{BI} |\Psi_{BI}^0\rangle |N_I/2, -N_I/2\rangle = 0$ and E_0 being the corresponding eigenenergy.

For $0 < t < \tau$, with τ denoting the exposure time, a rectangular pulse, $\Omega_{R0}(t) = \Omega_{R0} \theta(t) \theta(\tau - t)$ where θ is the heaviside theta function, induces Rabi oscillations between the spin- \uparrow ($g_{BI} \neq 0$) and spin- \downarrow ($g_{BI} = 0$) impurity states [4] in the course of time t , see Fig. 1

(b). In particular, for fixed Ω_{R0} the frequency of these Rabi oscillations depends on the detuning Δ following $\Omega_R = \sqrt{(Z\Omega_{R0})^2 + (\Delta - \Delta_+)^2}$ where Δ_+ is the resonance frequency associated with the Bose polaron formation characterized by a quasi-particle residue Z [3, 4]. The latter refers to the overlap between the initial non-interacting state $|\Psi_0\rangle$ of the system and the polaronic state $|\Psi_P\rangle$ after a single spin-flip, i.e. $Z = |\langle \Psi_0 | \hat{S}_x | \Psi_P \rangle|$. As we shall demonstrate below, the Rabi oscillations are damped due to the accumulation of spin-spatial correlations which are captured by the impurity-BEC complex. These correlations, in turn, lead to the decaying behavior of the polaron corresponding to $Z < 1$.

To monitor the above-described effects for different exposure times τ and variable detuning Δ , we resort to the fraction of impurity atoms that have been successfully transferred to the $|\uparrow\rangle$ -state [Fig. 1 (b)], namely

$$f(\Delta; \tau) = \frac{\langle N_\uparrow(t = \tau) \rangle}{N_I}, \quad (3)$$

where $N_I = N_\uparrow + N_\downarrow$. Due to the parabolic confinement, the timescale for the evolution of the spatial part of the MB wave function is given by $\sim \omega^{-1}$. The characteristic energy scale of the phononic excitations in the BEC is $\epsilon_{ph} = \hbar c/\xi$, where $c = \sqrt{g_{BB} n_B/m_B}$ denotes the speed of sound, $\xi = \hbar(2m_B g_{BB} n_B)^{-1/2}$ refers to the healing length and n_B is the peak density. The relevant timescale for impurity-medium correlations to develop is then, $t_{phI} = \xi/c \approx 0.08\omega^{-1}$. Moreover, the characteristic timescale for the evolution of the spin degrees of freedom is $t_0 \sim \Omega_{R0}^{-1}$, see Eq. (2) and Fig. 1 (b). As a consequence, there is a competition between the characteristic times of the spatial and spin evolution which affects the emergent correlation properties.

In particular, for $\Omega_{R0} \gg c/\xi \gg \omega$ (herein $c/\xi \approx 12.5$) the spatial MB wave function is unable to evolve during the short timescale, $T = 2\pi/(Z\Omega_{R0}) \approx t_0$, of the pulse-induced impurity Rabi oscillations. As such within this timescale, impurity-BEC correlations can hardly develop. This limiting case is referred to in the following as the *fully diabatic spin-transfer regime* [Fig. 1 (c)]. When $\Omega_{R0} \ll \omega \ll c/\xi$, on the other hand, the evolution of the spatial MB wave function is much faster than the impurity spin transfer, and we refer to a *fully adiabatic spin-transfer regime* [Fig. 1 (c)]. Here, the introduction of the rf pulse results in the transition from non-interacting (for spin- \downarrow impurities) to interacting (for spin- \uparrow impurities) eigenstates. Notice that the latter states are not necessarily the polaronic states e.g. due to the TOC phenomenon [25, 56].

Remarkably, within the intermediate spin-transfer regime characterized by $\omega < \Omega_{R0} < c/\xi$, the spatial correlations can build-up while effects due to the external confinement are suppressed. For these reasons, in the present work we are mainly interested in this intermediate regime of the rf pulse which essentially leads to a *locally adiabatic* transfer of the impurities where the

above-mentioned competition of timescales as defined by the trap (ω^{-1}) and the phononic excitations (ξ/c) is pronounced. The resultant polaron formation in the latter regime will be contrasted to the one emanating when approaching the diabatic limit for increasing Ω_{R0} .

B. Variational treatment of the spectral response

To address the rf spectroscopy of the above-discussed particle imbalanced multicomponent bosonic system we solve the underlying time-dependent MB Schrödinger equation by resorting to the ML-MCTDHX method [61, 62]. It constitutes a variational approach [73] for simulating the nonequilibrium quantum dynamics of bosonic and fermionic multicomponent spinor settings [24–26, 74]. More precisely, in order to capture the emergent impurity-BEC correlations, we first express the total MB wave function $|\Psi(t)\rangle$ as a linear combination of $k = 1, 2, \dots, D$ distinct orthonormal species functions, i.e. $|\Psi_k^\sigma(t)\rangle$ [61] for each individual component $\sigma = B, I$. This procedure results to a truncated Schmidt decomposition [75], possessing a rank D , which reads

$$|\Psi(t)\rangle = \sum_{k=1}^D \sqrt{\lambda_k(t)} |\Psi_k^B(t)\rangle |\Psi_k^I(t)\rangle. \quad (4)$$

The involved time-dependent expansion coefficients $\lambda_k(t)$ are termed Schmidt weights and are also known as the natural populations of the k -th species function. In particular, they correspond to the eigenvalues of the σ -component reduced density matrix i.e. $\rho_\sigma^{N_\sigma}(\vec{x}, \vec{x}'; t) = \langle \Psi(t) | \prod_{i=1}^{N_\sigma} \Psi_\sigma^\dagger(x_i) \prod_{i=1}^{N_\sigma} \Psi_\sigma(x'_i) | \Psi(t) \rangle$, with $\vec{x} = (x_1, \dots, x_{N_\sigma})$. By inspecting Eq. (4) it becomes also apparent that the system is entangled [76], and thus impurity-medium correlations are finite, when at least two different $\lambda_k(t)$ are nonzero; otherwise $|\Psi(t)\rangle$ is a direct product of two states and the system is non-entangled.

Subsequently, for incorporating the intracomponent correlations into the MB ansatz, each species function is expanded in terms of a time-dependent number-state basis set $|\vec{n}(\tau)\rangle^\sigma$ as follows

$$|\Psi_i^\sigma(t)\rangle = \sum_{\vec{n}} A_{i,\vec{n}}^\sigma(t) |\vec{n}(t)\rangle^\sigma. \quad (5)$$

Here, $A_{i,\vec{n}}^\sigma(t)$ denote the corresponding time-dependent expansion coefficients, while a particular number state $|\vec{n}(t)\rangle^\sigma$ refers to a permanent building upon d^σ time-dependent variationally optimized single-particle functions (SPFs). The latter read $|\phi_l^\sigma(t)\rangle$, $l = 1, 2, \dots, d^\sigma$ with $\vec{n} = (n_1, \dots, n_{d^\sigma})$ being the corresponding occupation numbers. Next, the SPFs are expressed on a time-independent primitive basis. For the bosonic medium this refers to an \mathcal{M} dimensional discrete variable representation (DVR) being designated by $\{|k\rangle\}$. Turning to the impurities this basis is the tensor product of the DVR

basis, $\{|k, s\rangle\}$, for the spatial degrees of freedom and the two-dimensional pseudospin-1/2 basis $\{|\uparrow\rangle, |\downarrow\rangle\}$. For our investigation $\mathcal{M} = 800$ grid points of a sine DVR are utilized. Therefore, a specific impurity SPF is a spinor wave function of the form

$$|\phi_j^I(t)\rangle = \sum_{k=1}^{\mathcal{M}} (B_{jk\uparrow}^I(t) |k\rangle |\uparrow\rangle + B_{jk\downarrow}^I(t) |k\rangle |\downarrow\rangle). \quad (6)$$

In this expression, the time-dependent expansion coefficients of the pseudospin- \uparrow [\downarrow] are $B_{jk\uparrow}^I(t)$ [$B_{jk\downarrow}^I(t)$], see also Refs. [25, 56] for a more elaborate discussion.

To determine the time-evolution of the underlying $(N_B + N_I)$ -body wave function $|\Psi(t)\rangle$ subjected to the Hamiltonian of Eq. (1) the so-called ML-MCTDHX equations of motion [61] are solved numerically. These are obtained by following the Dirac-Frenkel variational principle [77, 78] for the ansatz exemplified in Eqs. (4), (5) and (6) and results in a set of D^2 linear differential equations of motion regarding the $\lambda_k(t)$ coefficients being coupled to $D \left(\frac{(N_B + d^B - 1)!}{N_B! (d^B - 1)!} + \frac{(N_I + d^I - 1)!}{N_I! (d^I - 1)!} \right)$ and $d^B + d^I$ nonlinear integrodifferential equations for the species functions and the SPFs respectively.

Concluding, the main facet of this method is that it relies on the expansion of the system's MB wave function with respect to a time-dependent and variationally optimized basis which is accordingly tailored to account for all the important interparticle spatial and spin-spin correlations [73]. Simultaneously, the time-dependence of the basis enables for efficiently spanning the corresponding subspace of the Hilbert space at each time-instant for systems including mesoscopic particle numbers in different spatial dimensions [79, 80]. The Hilbert space truncation is signified by the used orbital configuration space, i.e. $C = (D; d^B; d^I)$. For the considered system the Bose gas comprises of a large number of weakly interacting atoms and as a consequence its intracomponent correlations are suppressed. Therefore, they can be captured by utilizing a small number of orbitals, here $d^B < 4$. On the contrary, since $N_I = 1, 2$, the number of integrodifferential equations is small which enables us to employ many orbitals, here $d^I = D = 8$, and thus account for strong impurity-impurity and impurity-medium correlations. Consequently, the amount of the underlying ML-MCTDHX equations of motion that should be evaluated is tractable.

C. Approximate spectral methods

1. Effective potential

To provide an intuitive understanding of the impurities spectral response and expose the necessity of including intra- and intercomponent correlations in the course of the evolution at least for certain intensities of the rf pulse we invoke an effective potential picture [49, 81] which has

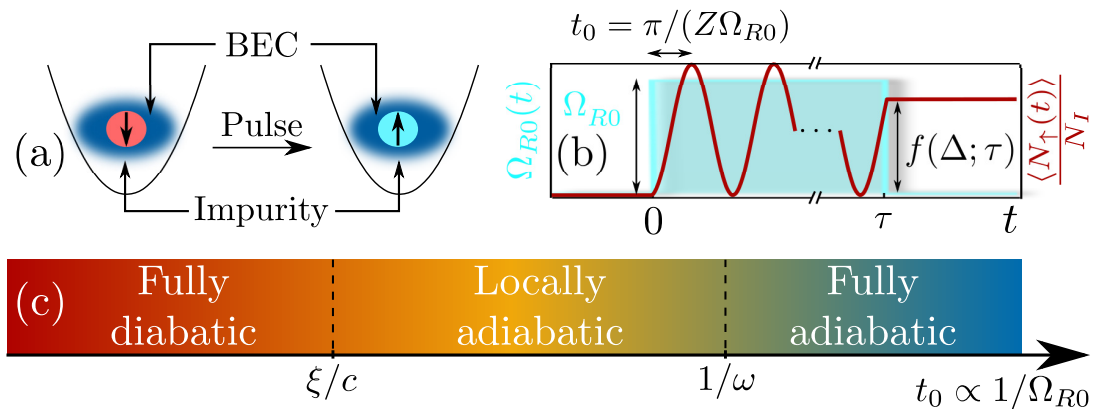


FIG. 1. (a) The impurity spin configuration before (left panel) and after (right panel) the application of the rectangular rf pulse. (b) Schematic representation of the utilized rectangular pulse (light-blue shaded region) imposed within the time-interval $0 < t < \tau$ and the expected time-evolution of the population of the spin- \uparrow atoms $\langle N_{\uparrow}(t) \rangle / N_I$ (red line) during the rf sequence. The spectroscopic signal $f(\Delta; \tau)$ is also illustrated [Eq. (3)]. (c) Categorization of the involved spin-transfer regimes as described by the characteristic timescale of the spin-dynamics t_0 in terms of the bare Rabi frequency Ω_{R0} (intensity) of the rf pulse. Here, ω denotes the external trapping frequency, c is the speed of sound, ξ the healing length of the BEC medium and Z refers to the polaron residue.

been shown to be adequate for $|g_{BI}| < g_{BB}$ [25, 45, 53]. It is constructed by the external harmonic oscillator and the density of the bosonic background accounting also for the characteristics of the pulse i.e. the bare Rabi frequency Ω_{R0} and detuning Δ . It essentially corresponds to a modified external harmonic potential and reads

$$\hat{V}_{eff}(g_{BI}) = \int dx \left\{ \left[\frac{1}{2} m_I \omega^2 x^2 + \frac{g_{BI}}{2} \rho_B^{(1)}(x) \right] \hat{\mathbb{I}}(x) + \left(\frac{g_{BI}}{2} \rho_B^{(1)}(x) - \frac{\hbar \Delta}{2} \right) \hat{S}_z(x) + \frac{\hbar \Omega_{R0}}{2} \hat{S}_x(x) \right\}, \quad (7)$$

where $\rho_B^{(1)}(x) \equiv \rho_B^{(1)}(x; g_{BI} = 0)$ refers to the ground state density of the medium [82] for vanishing impurity-BEC coupling strength ($g_{BI} = 0$) and $\hat{S}(x) = \sum_{ab} \hat{\Psi}_a^\dagger(x) \boldsymbol{\sigma}_{ab} \hat{\Psi}_b(x)$, $\hat{\mathbb{I}}(x) = \sum_a \hat{\Psi}_a^\dagger(x) \hat{\Psi}_a(x)$. As it can be readily seen, the form of $V_{eff}(x; g_{BI})$ implies that $\rho_B^{(1)}(x)$ acts on the impurities as an additional repulsive (for $g_{BI} > 0$) or attractive (if $g_{BI} < 0$) potential.

It is also worth mentioning that $V_{eff}(x; g_{BI})$ neglects several phenomena that might be important for the description of the impurity problem. In particular, $V_{eff}(x; g_{BI})$ disregards the impurity-medium correlations. Consequently, it does not include the renormalization of the impurity mass caused by the coupling with its environment and the possible emergence of impurity-impurity induced interactions due to the absence of two-body terms. Thus, it is naturally expected that two-body processes can not be captured within $V_{eff}(x; g_{BI})$. To track the nonequilibrium dynamics of the impurities within $V_{eff}(x; g_{BI})$ we solve the underlying time-dependent single-particle Schrödinger equation.

2. Diabatic approximation

Another interesting approximation that we shall employ in the following in order to unravel the impurity injection spectrum and importantly elucidate the transition to the *diabatic spin-transfer regime* where $\Omega_{R0} \gg c/\xi$ is the so-called diabatic approximation. As exemplified in Sec. II A, in this regime the spatial part of the MB wave function is not possible to adapt to the external perturbation within the small timescale of the pulse and hence the emergent impurity-medium correlations are expected to vanish. The main ingredient of the diabatic approximation is that in the course of the pulse the kinetic energy of the BEC and the impurities is considered to be negligible, and thus we treat the participating atoms as stationary ones during the application of the injection pulse. This can be understood by the fact that in the case of $\Omega_{R0} \gg c/\xi$ the impurities Rabi oscillation between their spin- \downarrow and spin- \uparrow states takes place at a much faster timescale i.e. $\sim 1/\Omega_{R0}$ as compared to the relative motion among the bath and the impurity atoms which is of the order of $\sim \xi/c$. The latter constitutes the characteristic timescale in which elementary BEC excitations form.

It can be systematically shown [see for details Appendix A] that within the diabatic approximation ($\Omega_{R0} \gg c/\xi > \omega$) the time-averaged rf signal, employing a second-order Taylor expansion in terms of Δ/Ω_{R0} , has the following form

$$\bar{f}(\Delta) = \frac{1}{2} \frac{\tilde{\Omega}^2}{\tilde{\Omega}^2 + \tilde{\Delta}^2} \left[1 + \frac{\tilde{\Delta}}{\tilde{\Omega}^2 + \tilde{\Delta}^2} + \frac{3}{8} \frac{3\tilde{\Delta}^2 - \tilde{\Omega}^2}{(\tilde{\Omega}^2 + \tilde{\Delta}^2)^2} + \mathcal{O} \left(\frac{\tilde{\Delta}^3}{(\tilde{\Omega}^2 + \tilde{\Delta}^2)^3}, \frac{\tilde{\Omega}^3}{(\tilde{\Omega}^2 + \tilde{\Delta}^2)^3} \right) \right]. \quad (8)$$

Here, $\tilde{\Omega}(\Omega_{R0}) = \frac{2g_{BB}\Omega_{R0}}{g_{BI}\omega}$ and $\tilde{\Delta}(\Delta) = \frac{2g_{BB}}{g_{BI}}[\frac{\Delta}{\omega} + \frac{1}{2}\frac{g_{BI}}{g_{BB}}(\frac{R_{TF}}{\alpha})^2]$ where $\alpha = \sqrt{\hbar/(m\omega)}$ is the harmonic oscillator length and R_{TF} is the Thomas-Fermi radius of the BEC background. It is worth mentioning that Eq. (8) implies that in the *adiabatic spin-transfer regime* the impurity spectrum corresponds to a Lorentzian. The latter is centered at $\tilde{\Delta}(\Delta_0) \approx -0.5$, or equivalently at $\Delta_0 \approx -\frac{\omega}{2}\frac{g_{BI}}{g_{BB}}\left[\left(\frac{R_{TF}}{\alpha}\right)^2 - \frac{1}{2}\right]$, and exhibits a half-width-at-half-maximum around $\gamma \approx \Omega_{R0}$. Importantly, we can readily deduce the linear dependence of the width of the peak γ on the used bare Rabi frequency Ω_{R0} . The origin of this result stems from the substantial power broadening of the rf spectrum for such high pulse intensities.

III. RADIOFREQUENCY SPECTRUM OF IMPURITIES IN A MASS-BALANCED MIXTURE

To probe the impurity excitation spectrum we theoretically simulate the celebrated technique of reverse rf spectroscopy [7, 17, 57]. The dynamical protocol characterizing this spectroscopic scheme consists of the following steps. Initially the multicomponent bosonic system satisfying the MB Hamiltonian of Eq. (1) is prepared in its ground state with zero impurity-medium interaction strength i.e. $g_{BI} = 0$, a bare Rabi coupling Ω_{R0} and vanishing detuning $\Delta = 0$. Particularly, the BEC medium of $N_B = 100$ atoms resides in its interacting ground state with $g_{BB} = 0.5$ and thus having a Thomas-Fermi radius $R_{TF} \approx 4.2$. The single as well as the two non-interacting bosonic impurities lie in their spin- \downarrow (ground) state where $g_{B\downarrow} = 0$.

To trigger the impurity nonequilibrium dynamics a rectangular rf pulse of a specific bare Rabi frequency Ω_{R0} and varying detuning Δ for different realizations is subsequently applied, thus driving the impurity atoms to their interacting spin- \uparrow state. Importantly, we study the resulting spectral response at specific impurity-medium couplings g_{BI} for different Ω_{R0} with respect to Δ in order to understand the emergent correlation phenomena of the induced spin-flip dynamics and also categorize the latter at distinct spin-transfer regimes ranging from the adiabatic to the diabatic limit. More precisely, below, we focus on three different values of g_{BI} being representative of the formation of repulsive ($g_{BI} = 0.5$) and attractive ($g_{BI} = -0.5$) Bose polarons satisfying $|g_{BI}| \leq g_{BB}$ as well as at strong repulsions ($g_{BI} = 1.5$) i.e. $g_{BI} > g_{BB}$ yielding a dynamical decay of the emergent quasi-particle [25]. The existence and stability of these states has been recently theoretically probed utilizing Ramsey [25, 53] and pump-probe spectroscopy [56].

As explicated in Sec. II A the simulated spectroscopic signal presented for instance in Fig. 2 corresponds to the fraction of impurity atoms $f(\Delta; \tau)$ [Eq. (3)] that have been successfully transferred to the spin- \uparrow state. The applied rectangular pulses [Fig. 1 (b)] being abruptly

switched on (off) at time $t = 0$ ($t = \tau$) are characterized by fixed Ω_{R0} , varying detuning Δ and pulse time τ . The participating frequencies in $f(\Delta; \tau)$ are estimated by measuring the Fourier transform of the spectrum $f(\Delta; \Omega_R) = \int_0^T d\tau f(\Delta; \tau)e^{i\Omega_R\tau}$ with $T = \max(\tau)$ being the duration of the most extensive pulse. Moreover, in order to facilitate a comparison between the spectral responses at different intensities of the rf pulse and approximations we also invoke the time-averaged transfer fraction over $0 < \tau < T$ being defined as $\bar{f}(\Delta) = (1/T) \int_0^T d\tau f(\Delta; \tau)$.

To reveal the spatially resolved dynamics of the spin- \uparrow and spin- \downarrow impurity state as well as of the BEC medium we monitor the one-body reduced density matrix for each component [83], namely

$$\rho_\sigma^{(1)}(x, x'; t) = \langle \Psi(t) | \hat{\Psi}_\sigma^\dagger(x) \hat{\Psi}_\sigma(x') | \Psi(t) \rangle. \quad (9)$$

Here, $\hat{\Psi}_\sigma(x)$ is the $\sigma = B, \uparrow, \downarrow$ -component bosonic field operator acting at position x and obeying the standard bosonic commutation relations [72]. In the following, we will inspect the respective one-body densities of each component i.e. $\rho_\sigma^{(1)}(x; t) \equiv \rho_\sigma^{(1)}(x, x' = x; t)$. Recall that this quantity is experimentally accessible via averaging over a sample of single-shot images [74, 84].

A. Multimode dynamics of coherent repulsive Bose polaron

Considering a bare Rabi frequency $\Omega_{R0} = \omega = 1 \ll c/\xi$ and for fixed repulsive impurity-BEC interactions $g_{BI} = 0.5$, the obtained rf signal with varying Δ and pulse time t is showcased in Fig. 2 (a). Evidently, a resonance occurs for $\Delta_+^* = -8.5$ having three predominant Rabi frequencies, i.e. $\Omega_R \approx 1.05$, $\Omega_R \approx 0.63$ and $\Omega_R \approx 0.44$, see the inset of Fig. 2 (a). The former signifies the existence of a repulsive Bose polaron [3, 23, 53]. Notice here that $V_{eff}(x; g_{BI})$ for the spin- \uparrow impurity is proximal to a square well of length $2R_{TF}$ [53]. Therefore, its lowest lying states possess energies $\epsilon_n \approx \epsilon_0 + n^2\pi^2\hbar^2/[2m_I(2R_{TF})^2] \approx \epsilon_0 + 0.0554\hbar\omega n^2$ with n indexing each eigenstate. This implies that the involved energy differences are much smaller than $\Omega_{R0} = 1$ and as a consequence the pulse acts almost diabatically on the impurity forming a superposition of the above-mentioned states. Indeed, monitoring the impurity spin densities we observe that $\rho_\uparrow^{(1)}(x; t)$ features a double and three peaked structure during the dynamics while expanding and contracting [Fig. 3 (a)] within its bosonic environment. Moreover, a multimode spin-transfer process between the $|\downarrow\rangle$ and $|\uparrow\rangle$ states occurs, containing the previously identified frequencies, due to the complex expansion dynamics of the spin- \uparrow impurity portion. This multifrequency character is also imprinted in the dynamics of $\rho_\downarrow^{(1)}(x; t)$ majorly residing at $x \approx 0$ [Fig. 3 (b)]. The respective medium only shows marginal distortions, see the inset of Fig. 3 (a), referring to weakly excited

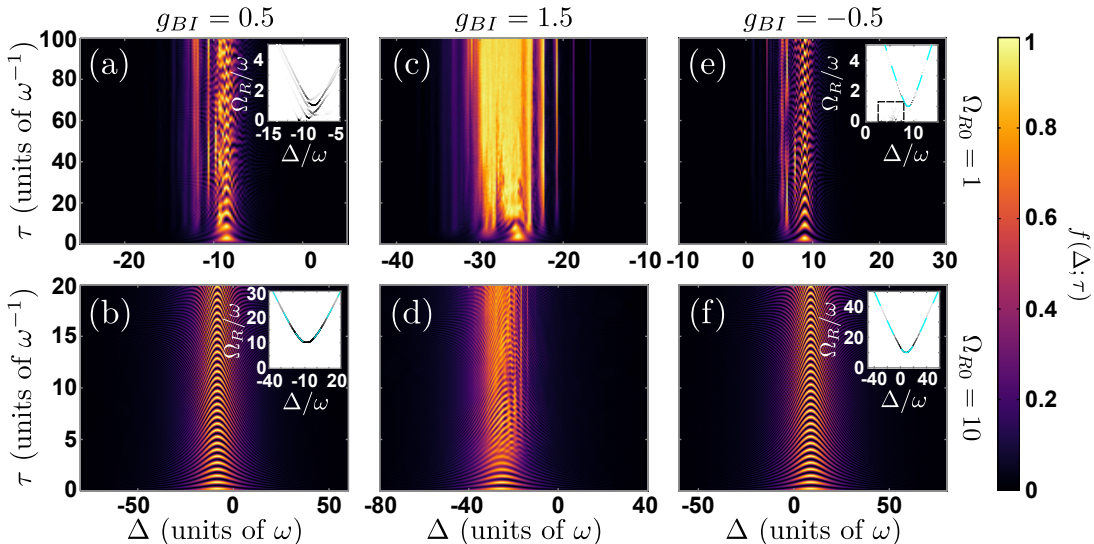


FIG. 2. Temporal evolution of the spectroscopic signal $f(\Delta; \tau)$ of a single impurity $N_I = 1$, featuring multiple polaronic resonances, with respect to the detuning of the rf field and different impurity-bath couplings for a bare Rabi frequency (a), (c), (e) $\Omega_{R0} = 1$ and (b), (d), (f) $\Omega_{R0} = 10$. In particular, we consider (a), (b) $g_{BI} = 0.5$, (c), (d) $g_{BI} = 1.5$, and (e), (f) $g_{BI} = -0.5$ corresponding to the cases of repulsive Bose polaron, its dynamical decay (TOC) and the attractive polaron regimes respectively. The insets provide the corresponding Fourier spectrum of the signal $f(\Delta; \Omega_R)$. The dashed light-blue line in the insets of (b), (e), (f) constitutes a fitting of the theoretically anticipated $\Omega_R = \sqrt{(Z\Omega_{R0})^2 + (\Delta - \Delta_+^*)^2}$, with Δ_+^* being the position of the resonance and $Z \approx 0.98$ [$Z \approx 0.99$] is the quasi-particle residue in (b) [(e), (f)]. The dashed box in the inset of (e) marks the presence of frequencies Ω_R corresponding to the spectral peaks at $\Delta < \Delta_+^*$. In all cases the mass-balanced ($m_B = m_I$) and harmonically trapped ($\omega = 1$) system consists of $N_B = 100$ bosons with $g_{BB} = 0.5$ and a single impurity where $g_{B\downarrow} = 0$.

phononic modes stemming from the polaron formation and dynamics.

Other resonances taking place at smaller detunings, e.g. for $\Delta_+ \approx -9.2$, $\Delta_+ \approx -10.6$ and $\Delta_+ \approx -12$, correspond to polaronic states with an excited motional degree-of-freedom, see also Fig. 4 (a). Indeed, for a trapped system these states have a discrete (quantized) spectrum in contrast to the homogeneous case where the momentum of the polaron is a real-valued good quantum number [4, 21, 38]. They exhibit a much lower Ω_R when compared to the $\Delta_+ = -8.5$ case. This decrease of Ω_R is due to the smaller overlap, or equivalently residue, of the excited polaronic states with the initial non-interacting one and it can be also inferred by the slow spin-transfer dynamics [Figs. 3 (e), (f)]. In particular, these states are related to superpositions of energetically higher-lying eigenstates of $V_{eff}(x; g_{BI})$ introduced in Sec. II C 1, see also the discussion in Refs. [25, 53]. Indeed, by inspecting the time-averaged spectrum $\bar{f}(\Delta)$ [Fig. 4 (a)] the locations of the above-discussed resonant peaks are adequately captured by $V_{eff}(x; g_{BI})$ [Eq. (7)]. A clear manifestation of the character of these states appears in the evolution of $\rho_{\uparrow}^{(1)}(x; t)$ shown in Fig. 3 (e) for $\Delta_+ = -10.6$. Evidently, $\rho_{\uparrow}^{(1)}(x; t)$ exhibits a multi-hump structure, indicative of the higher-lying excitations participating in the dynamics at these detunings. Additionally, the bosonic bath [inset of Fig. 3 (f)] is only slightly perturbed due to the sound wave emission asso-

ciated with the polaronic excitations [45, 85].

The remaining resonant peaks identified in the spectrum and are not present within $V_{eff}(x; g_{BI})$ [Fig. 4 (a)], for instance the peak at $\Delta_+ = -9.8$ [see the arrow in Fig. 4 (a)], occur as a result of the coupling of the polaron resonances with the collective background excitations [53, 64]. The latter refer majorly here to a breathing mode, see in particular the dynamics of $\rho_B^{(1)}(x; t)$ in the inset of Fig. 3 (d). As expected, an underlying spin-mixing dynamics among the impurity spin components, see Figs. 3 (c), (d), takes place with the $\rho_{\uparrow}^{(1)}(x; t)$ spreading within the BEC background and having a multinodal shape. Interestingly, within the time-interval ($25 < t < 75$) where the $|\uparrow\rangle$ state is maximally occupied the bosonic medium undergoes a pronounced breathing mode.

Moreover, by comparing $\bar{f}(\Delta)$ between the MB scenario and the diabatic approximation, see Fig. 4 (a), we can deduce that for $\Omega_{R0} = 1$ the pulse intensity is not sufficient to reach the diabatic spin-transfer regime since the two spectra differ substantially. Interestingly, $\bar{f}(\Delta)$ as obtained in the MB approach for two non-interacting bosonic impurities almost coincides with the one of $N_I = 1$ [Fig. 4 (a)]. The latter suggests that here the emergent polaronic peaks are predominantly of single-particle character, a result that will be further analyzed and differences will be exposed later on in Sec. IV. However, by merely inspecting $\bar{f}(\Delta)$ the most essential

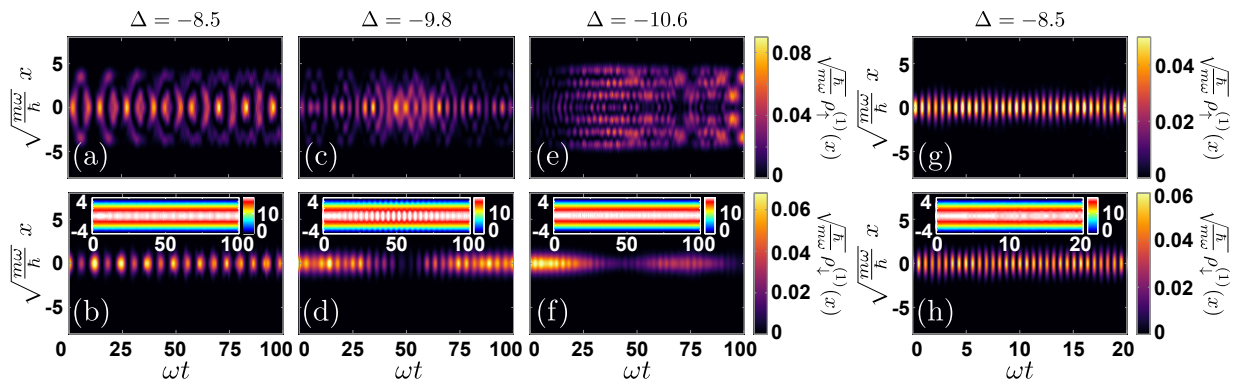


FIG. 3. Spatiotemporal evolution of the single-particle density (a), (c), (e) $\rho_{\uparrow}^{(1)}(x;t)$ (spin- \uparrow) and (b), (d), (f) $\rho_{\downarrow}^{(1)}(x;t)$ (spin- \downarrow) of a single impurity for different detunings Δ of the rf field (see legends) and fixed bare Rabi frequency $\Omega_{R0} = 1$. The repulsive g_{BI} leads to a delocalization trend of the impurity density indicating its excited nature. The insets of (b), (d), (f) present the corresponding density evolution $\rho_B^{(1)}(x;t)$ of the bosonic background where phononic excitations are imprinted. (g) $\rho_{\uparrow}^{(1)}(x;t)$ and (h) $\rho_{\downarrow}^{(1)}(x;t)$ of a single impurity for $\Delta = -8.5$ and $\Omega_{R0} = 10$ featuring a more localized behavior than $\Omega_{R0} = 1$ due to the faster spin dynamics. The respective $\rho_B^{(1)}(x;t)$ is showcased in the inset of (h). In all cases $g_{B\downarrow} = 0$ and $g_{B\uparrow} \equiv g_{BI} = 0.5$. The remaining system parameters are the same as in Fig. 2. The pulse time in (a)-(f) $\tau = T = 100 > t$ while in (g), (h) $\tau = T = 20 > t$. The Thomas-Fermi radius of the BEC medium is $R_{TF} \approx 4.2$.

difference between the $N_I = 2$ and $N_I = 1$ impurities is that in the former case the amplitude of the higher-lying peak at $\Delta_+ \approx -10.6$ is larger. This alteration is caused by the larger number of impurities where the amount of excitations is enhanced.

Turning to a more intense rf pulse with $\omega < \Omega_{R0} = 10 < c/\xi \approx 12.5$ (intermediate spin-transfer regime, Fig. 1 (c)) and for $g_{BI} = 0.5$ it becomes apparent that the spectral response shows a central polaronic resonance around $\Delta_+^* \approx -9.2$ [Fig. 2 (b)]. It is also characterized by a single Rabi frequency which satisfies the relation $\Omega_R(\Delta) = \sqrt{(Z\Omega_{R0})^2 + (\Delta - \Delta_+^*)^2}$ with respect to Δ , see the inset of Fig. 2 (b) where $Z \approx 0.98$. The impurity simply Rabi oscillates between its spin- \downarrow and spin- \uparrow states as it can easily be inferred by monitoring its spin densities evolution presented in Fig. 3 (g), (h) exemplarily for $\Delta = \Delta_+^*$. Note that weak amplitude sound waves are accordingly imprinted onto the density of the BEC background [85, 86] caused by the impurity motion in the latter [inset of Fig. 3 (h)]. Furthermore, the respective time-averaged signal $\bar{f}(\Delta)$ has the form of a Lorentzian distribution for both one and two bosonic impurities, a result that is further supported by its almost perfect agreement with $\bar{f}(\Delta)$ as predicted by the diabatic approximation [Fig. 4 (b)]. The latter implies that within the dynamics for $\Omega_{R0} = 10$ the diabatic spin-transfer regime has already been reached, despite the fact that $\Omega_{R0} < c/\xi$. Also, since $\bar{f}(\Delta)$ is unaltered for $N_I = 1$ and $N_I = 2$ it means that two-body processes are not manifest. In this limit the effective potential leads to exactly the same shape of $\bar{f}(\Delta)$, suggesting that impurity-BEC correlations are suppressed.

The crossover from the adiabatic to the diabatic spin-transfer regime imprinted in the rf signal can be visualized in terms of the structural change of $\bar{f}(\Delta)$ for in-

creasing Ω_{R0} , see Fig. 5 (a). Evidently, for $\Omega_{R0} \leq \omega$ the averaged spectrum $\bar{f}(\Delta)$ features a main polaronic resonance e.g. at $\Delta_+^* \approx -8.45$ [$\Delta_+^* \approx -8.5$] while secondary ones signifying higher-order polaronic excitations appear at smaller detunings for instance at $\Delta_+ \approx -8.8$, $\Delta_+ \approx 9.65$ [$\Delta_+ \approx -10.6$, $\Delta_+ \approx -12$] for $\Omega_{R0} = 0.1$ [$\Omega_{R0} = 1$]. We remark that the number of these secondary resonances is smaller for decreasing $\Omega_{R0} \leq \omega$ since in the latter case the pulse is less intense and thus prohibits the spectral resolution of the higher-lying motional states of the polaron possessing $Z \ll 1$. Recall that the resonance peak for a rectangular pulse when $\Omega_{R0} \ll \omega$ is $f(\Delta_+; \tau) \sim \sin^2(Z\Omega_{R0}\tau/2)$ [56] and thus low residue peaks cannot manifest within the timescale considered herein. In sharp contrast if $\omega \ll \Omega_{R0} < c/\xi$ even though the locally adiabatic regime is expected [Fig. 1 (c)] the system exhibits a fully diabatic behavior as captured by $\bar{f}(\Delta)$ [Fig. 4 (b)]. Indeed, the latter possesses a Lorentzian distribution whose width is enhanced for a larger Ω_{R0} due to power broadening, see also Eq. (8). Here, $\bar{f}(\Delta)$ shows a single polaronic resonance with an Ω_{R0} -dependent location for fixed g_{BI} . The above indicate that the impurity-bath coupling is adequately weak and therefore the impurity-phonon correlations can not affect the spin dynamics triggered by such intense pulses.

B. Emergence of temporal orthogonality catastrophe

We now discuss the emergent rf response for strong repulsive coupling, and in particular for $g_{BI} = 1.5 > g_{BB}$. The rf signal $f(\Delta; \tau)$ upon applying a pulse with $\Omega_{R0} = \omega = 1 \ll c/\xi$ and varying detuning is demonstrated in Fig. 2 (c). A multitude of spectral peaks is

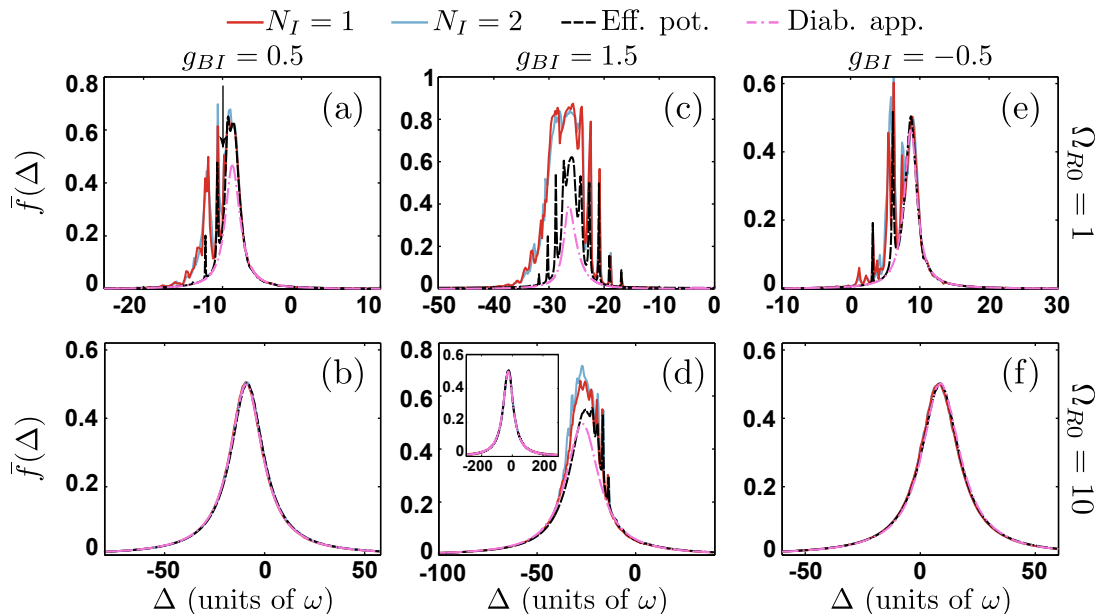


FIG. 4. Time-averaged spectroscopic signal $\bar{f}(\Delta)$ of a single ($N_I = 1$) and two ($N_I = 2$) bosonic non-interacting ($g_{\uparrow\uparrow} = 0$) impurities and within different approaches (see legend). The cases of adiabatic (a), (c), (e) $\Omega_{R0} = 1$ and diabatic (b), (d), (f) $\Omega_{R0} = 10$ spin-transfer regimes are depicted for interactions resulting to the formation of (a), (b) repulsive $g_{BI} = 0.5$, (e), (f) attractive $g_{BI} = -0.5$ and (c), (d) the dynamical decay $g_{BI} = 1.5$ of the Bose polaron. The inset in (d) shows $\bar{f}(\Delta)$ for $\Omega_{R0} = 40$. The arrow in (a) indicates the spectral peak referring to the mode-coupling of the polaron with the collective background excitations. Other system parameters are the same as in Fig. 2.

observed in $f(\Delta; \tau)$ with the latter featuring a saturation tendency during the dynamics and in particular for $\tau > 40$. This saturation trend together with the appearance of the multiple peaks in $f(\Delta; \tau)$ are clear manifestations of the dynamical decay, and consequently vanishing residue, of the emergent quasi-particle and its associated TOC phenomenon [25, 56]. The latter is caused by the build up of strong impurity-BEC correlations leading to the impurity dephasing and phase separation from the bosonic medium, as we shall show below.

The time-averaged spectrum $\bar{f}(\Delta)$ shown in Fig. 4 (c) reveals the appearance of several resolved narrow peaks for $\Delta > -25$. Additionally a broad, i.e. possessing a width much larger than $\Omega_{R0} = 1$, continuous distribution of excitations for $\Delta < -25$ occurs. The nature of these spectral features can be identified by contrasting the $\bar{f}(\Delta)$ for $N_I = 1$ with the corresponding one obtained within the effective potential approximation. Notice that the dynamics within $V_{eff}(x; g_{BI})$ cannot capture the phenomenon of TOC and is characterized by coherent evolution. Within this approximation, the spectrum is dominated by a prominent and power broadened peak at $\Delta_+^* \approx -25.8$, with additional individual narrower resonances for both larger and smaller detuning. For such strongly repulsive impurity-bose coupling, the potential $V_{eff}(x; g_{BI})$ for the spin- \uparrow impurities possesses a double-well structure. The eigenstates corresponding to $\Delta_+^* \approx -25.8$ possess eigenenergies of the order of the barrier height and accordingly have a prominent single-particle density within the spatial extent of the bar-

rier, i.e. within the BEC [53]. Similarly to the case of $g_{BI} = 0.5$, the energy levels of those states are closely packed and therefore the pulse acts almost diabatically creating a superposition. In contrast, the states of lower energy i.e. $\Delta > -25$ mainly reside in the periphery of the cloud at $x \approx R_{TF}$, while the states with $\Delta < -26$ show a highly multinodal structure implying the contribution of large impurity momenta.

The structure of $\bar{f}(\Delta)$ for $N_I = 1$ can be understood by relying on the above-mentioned features of $V_{eff}(x; g_{BI})$. In particular, it is known [25, 53] that the TOC occurs when the superfluidity of the BEC breaks due to rapidly moving impurities within its spatial extent that transfer their energy to the host by phonon emission. Accordingly, the spin- \uparrow states created by an rf pulse with $\Delta > -25$ do not possess a large density overlap with the BEC and the TOC is not pronounced [see Fig. 6 (c) for $\Delta = -20.8$]. This fact permits their resolution as individual peaks in $\bar{f}(\Delta)$ for $N_I = 1$ [Fig. 2 (c) for $\Delta = -21$]. Notice that their larger amplitude when compared to the $V_{eff}(x; g_{BI})$ spectrum is attributed to their eventual but rather slow evolving TOC resulting in the population trapping of the impurity in the spin- \uparrow state due to the transfer of the impurity energy to the background [Fig. 7 (a)]. The situation is radically different for $\Delta \leq -25$ though, since in this case the transferred spin- \uparrow impurities lie within the spatial extent of the BEC and are subsequently accelerated towards the periphery of the cloud due to $V_{eff}(x; g_{BI})$ [see Fig. 6 (a) for $\Delta = -25.8$ and $t < 10$]. This process results in a pronounced and

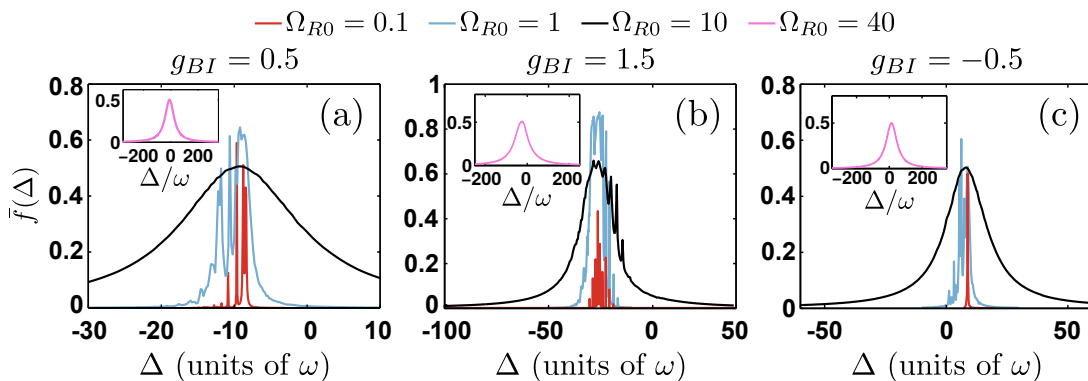


FIG. 5. Time-averaged spectroscopic signal $\bar{f}(\Delta)$ for varying detuning Δ and different impurity-medium interactions g_{BI} as well as bare Rabi frequencies Ω_{R0} (see legends) in the MB case. The insets represent the $\bar{f}(\Delta)$ for $\Omega_{R0} = 40$. The crossover from adiabatic to diabatic spin-transfer is realized for an increasing Ω_{R0} and fixed g_{BI} being captured by the modification of $\bar{f}(\Delta)$ from a multiple peaked structure to a Lorentzian shape. The remaining system parameters are the same as in Fig. 2.

rapidly evolving TOC and leads to the accumulation of the spin- \uparrow impurities outside of the Thomas-Fermi radius, implying $f(\Delta, \tau) \rightarrow 1$ for large evolution times ($t > 25$) and consequently $\bar{f}(\Delta)$ is enhanced. Notice also that TOC is not spectrally selective as it appears as long as particles are transferred to the spin- \uparrow state [Fig. 2 (c) for $\tau > 10$] and it is insensitive to the detuning from the resonance yielding a broad distribution instead of individual peaks [Fig. 4 (c)]. This fact can be attributed to the rapid character of the TOC which occurs at a fast timescale of ω^{-1} as it has been recently revealed by pump-probe spectroscopy [56].

The additional spectral peaks identified in $\bar{f}(\Delta)$ for $\Delta < -26$ within $V_{eff}(x; g_{BI})$ [Fig. 4 (c)] possess a secondary role. Indeed, the increased transfer rate to the spin- \uparrow state associated with them results in a more efficient expulsion of the impurity from the spatial extent of the BEC [Fig. 6 (a)]. This process leads to a local maximum in $f(\Delta)$ within the region of the continuum distribution of excitations. Turning our attention to $\bar{f}(\Delta)$ for $N_I = 2$, we observe an almost perfect match with the spectrum of $N_I = 1$. Small aberrations for $\Delta \leq -26$ can be attributed to a blockade-like phenomenon occurring during the dynamics which will be analyzed in Sec. IV. Let us note in passing that the kinetic energy of the impurities plays a crucial role in determining the spectral response of the system for $\Omega_{R0} = 1$. As such, the diabatic approximation fails completely to capture the spectral features exhibited for such intensities of the rf pulse [Fig. 4 (c)].

In order to visualize the impurity behavior we investigate the spatiotemporal evolution of its spin densities within the MB method, see Figs. 6 (a)-(d). Focusing on $\Delta_+^* = -25.8$ [Figs. 6 (a)-(b)] we observe the two transfer cycles of the impurity from its spin- \downarrow to the spin- \uparrow state and vice versa until $t \approx 12$. Afterwards the impurity remains trapped in its spin- \uparrow state whilst the spin- \downarrow one is almost completely depopulated. At the initial pulse times a Gaussian-like density hump builds upon $\rho_{\uparrow}^{(1)}(x; t)$

residing around $x = 0$ which subsequently splits into two fragments that are symmetrically placed with respect to $x = 0$ and support a multihump shape. Remarkably, these impurity density fragments execute a damped oscillatory motion during the pulse time and are located around the edges of the Thomas-Fermi radius of the BEC background, a process that gives rise to an impurity-medium phase-separation and accordingly leads to the TOC [25, 53]. A similar phenomenology occurs also for other detuning corresponding to the remaining spectral resonances, see e.g. the time-evolution of the involved spin densities at $\Delta_+ = -20.8$ depicted in Figs. 6 (c)-(d). Apparently, a much slower impurity transfer is achieved from the $|\downarrow\rangle$ to the $|\uparrow\rangle$ states with $\rho_{\downarrow}^{(1)}(x; t)$ lying at the trap center. However, also in this case, after the initial population of the $|\uparrow\rangle$ configuration by an impurity portion two density branches appear in $\rho_{\uparrow}^{(1)}(x; t)$ which undergo damped amplitude oscillations being centered at the edges of the Thomas-Fermi background. Notice here the humped structure of $\rho_{\uparrow}^{(1)}(x; t)$ which possesses a smaller number of nodes compared to $\Delta_+^* = -25.8$ indicating the lower excitation order of the impurity in the former case.

The above-described TOC phenomenon is inherently related to a migration of the impurity energy into the BEC medium [56, 85, 87]. This process can be directly verified by investigating the expectation value of the energy of the bosonic gas during the time-evolution, namely $E_B(t) \equiv \langle \Psi(t) | \hat{H}_B^0 + \hat{H}_{BB} | \Psi(t) \rangle$, see also Eq. (1). The behavior of $E_B(t) - E_B(0)$ is presented in Fig. 7 for $\Omega_{R0} = 1$ and different detunings Δ of the rf field corresponding to specific resonant peaks identified in $\bar{f}(\Delta)$. Clearly the energy of the bath evinces an overall increasing tendency in the course of the pulse time implying an energy transfer from the impurity to its background. Of course, the respective impurity-BEC interaction energy i.e. $E_{BI}^{int}(t) \equiv \langle \Psi(t) | \hat{H}_{BI}^{int} | \Psi(t) \rangle$ simultaneously decreases (not shown here). The rate and amount of energy migration is more prominent for resonances char-

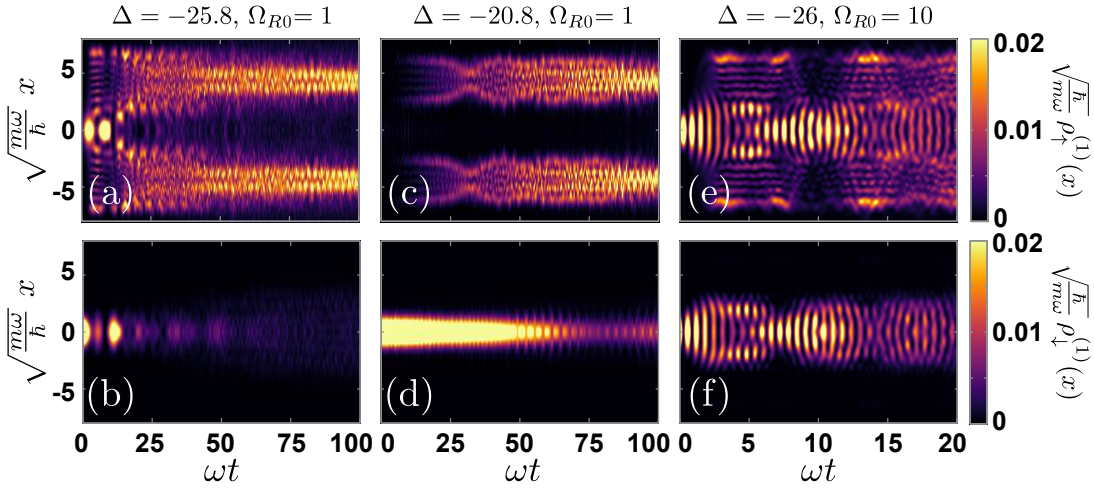


FIG. 6. Density evolution (a), (c), (e) $\rho_{\uparrow}^{(1)}(x;t)$ (spin- \uparrow) and (b), (d), (f) $\rho_{\downarrow}^{(1)}(x;t)$ (spin- \downarrow) of a single impurity for varying detuning Δ (see legends) and bare Rabi frequency (a)-(d) $\Omega_{R0} = 1$ and (e), (f) $\Omega_{R0} = 10$. It holds that $g_{B\downarrow} = 0$ and $g_{B\uparrow} \equiv g_{BI} = 1.5$, whilst the remaining parameters are the same to the ones considered in Fig. 2. The dynamics in (a)-(d) of the impurity spin- \uparrow density manifests the TOC phenomenon accompanied by the depletion of the spin- \downarrow state (see text). For $\Omega_{R0} = 10$ the emergent Rabi oscillations are faster compared to the timescale where the impurity escapes the background, thus approaching the locally adiabatic spin-transfer regime. The considered pulse time corresponds to (a)-(d) $\tau = T = 100 > t$ and (e), (f) $\tau = T = 20 > t$. The Thomas-Fermi radius of the bosonic gas corresponds to $R_{TF} \approx 4.2$.

acterized by a larger magnitude of detuning such that $\Delta_{+} \rightarrow \Delta_{+}^{*} \approx -26$ since it essentially yields a more significant spatial overlap of the involved metastable polaron state and the bath [88]. This increased overlap leads to a more rapid TOC and therefore transfer of the impurity energy to the bath. It is also worth mentioning that $E_B(t) - E_B(0)$ features certain amplitude oscillations which are attributed to the ‘‘collisions’’ of $\rho_{\uparrow}^{(1)}(x;t)$ with $\rho_B^{(1)}(x;t)$ during the phase-separation process [25]. Moreover, keeping fixed the detuning e.g. to $\Delta_{+}^{*} = -26$ and considering a larger bare Rabi frequency leads to a smaller amount of energy transfer into the bath. This can be understood since the enhancement of Ω_{R0} , and thus of the pulse amplitude, essentially gives rise to a faster spin-transfer which naturally does not let the impurity to adapt to modified coupling with the environment [4, 58].

To appreciate the reduced degree of coherence already indicated by the rf spectrum we rely on the time-average over the entire evolution (T), see also the discussion below Eq. (9), of the spatial first-order coherence function

$$\bar{g}_{\sigma}^{(1)}(x, x') = \frac{1}{T} \int_0^T dt \frac{\rho_{\sigma}^{(1)}(x, x'; t)}{\sqrt{\rho_{\sigma}^{(1)}(x; t) \rho_{\sigma}^{(1)}(x'; t)}}. \quad (10)$$

In this expression, $\rho_{\sigma}^{(1)}(x, x'; t)$ refers to the $\sigma = B, \uparrow, \downarrow$ component one-body reduced density matrix [Eq. (9)] whose diagonal is the one-body density i.e. $\rho_{\sigma}^{(1)}(x; t)$. Evidently, $|\bar{g}_{\sigma}^{(1)}(x, x'; t)| \in [0, 1]$ reveals the spatially resolved deviation of a MB wave function from a corresponding product state. In particular, when $|\bar{g}_{\sigma}^{(1)}(x, x')| = 1$ the component is called fully coherent

otherwise coherence losses come into play exposing the build up of correlations [74]. We remark that initially ($t = 0$) both the impurity and the environment are almost fully coherent (not shown for brevity). Inspecting $|\bar{g}_B^{(1)}(x, x')|$ in the case of $\Omega_{R0} = 1$ dictates that in the bosonic gas a small amount of coherence losses occur as can be inferred from the corresponding off-diagonal since e.g. $|\bar{g}_B^{(1)}(x = -4, x' = 4)| \approx 0.85$ [Fig. 7 (b)]. However, regarding the impurity we can readily deduce the occurrence of substantial coherence losses being evident by the fade out of $|\bar{g}_{\uparrow}^{(1)}(x, x' \neq x)| \rightarrow 0$ [Fig. 7 (c)] and therefore any polaronic notion is lost as also probed by the rf spectra [Fig. 2 (c)]. A similar conclusion has also been unveiled recently by monitoring the polaronic spectrum using a pump-probe spectroscopic scheme [56].

Increasing the bare Rabi frequency, namely $\omega \ll \Omega_{R0} = 10 < c/\xi$, results in a modified spectral response $f(\Delta; \tau)$ [Fig. 2 (d)] and therefore time-averaged rf spectrum $\bar{f}(\Delta)$ [Fig. 4 (d)]. In the course of the pulse time $f(\Delta; \tau)$ initially ($t < 4$) performs single frequency Rabi oscillations and later on features a multifrequency behavior [Fig. 2 (d)]. Several resonant peaks e.g. at $\Delta_{+} \approx -26$, $\Delta_{+} \approx -20$, $\Delta_{+} \approx -17.3$ and $\Delta_{+} \approx -14.5$ appear in both $f(\Delta; \tau)$ and $\bar{f}(\Delta)$ designating motionally excited polaronic states formed by the partially dressed portion of the spin- \uparrow impurity. This partial dressing mechanism of the impurity can be directly inferred from the spatially resolved evolution of the spin densities, see for instance Figs. 6 (e), (f). Indeed, at the initial stages of the dynamics ($t < 2.5$) a fast Rabi-type transfer of atoms from the spin- \uparrow to the spin- \downarrow state and vice versa occurs causing an undulation to the BEC density in the vicin-

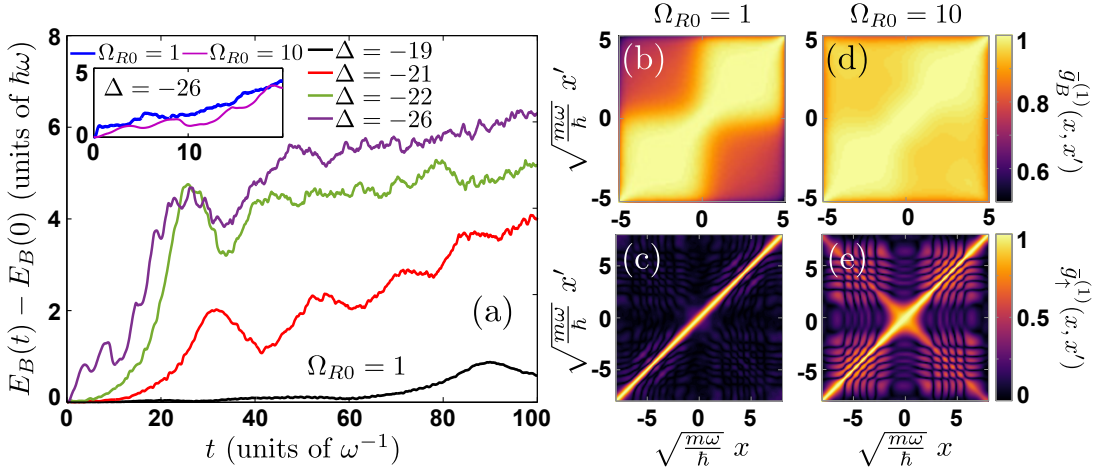


FIG. 7. Dynamics of the expectation value of the energy of the bosonic medium, $E_B(t) - E_B(0)$, for different detunings Δ (see legend), fixed Rabi frequency of the rf field $\Omega_{R0} = 1$ and pulse time $\tau = T = 100 > t$. The observed increasing behavior with time showcases the energy transfer from the impurity to the BEC medium. The inset shows $E_B(t) - E_B(0)$ for constant $\Delta = -26$ and distinct values of Ω_{R0} (see legend). Time-averaged one-body coherence function of (b), (d) the bosonic medium and (c), (e) the impurity for varying Ω_{R0} (see legend) and fixed $\Delta = -26$ demonstrating coherence losses due to the TOC phenomenon. In all cases, $g_{B\downarrow} = 0$, $g_{B\uparrow} \equiv g_{BI} = 1.5$ and the remaining parameters are the same as in Fig. 2.

ity of $\rho_{\uparrow}^{(1)}(x;t)$ within $\Omega_{R0}^{-1} > \xi/c$. Notice that in the short time-interval where the impurity is excited to the spin- \uparrow state ($\sim \pi/\Omega_{R0} \approx 0.3 < \omega$) it can hardly disperse until it is de-excited to the spin- \downarrow state. Due to this non-dispersive character of $\rho_{\uparrow}^{(1)}(x;t)$ in each Rabi-cycle the impurity interacts stronger with the emitted BEC excitations (phonons) leading to its larger spatial localization in the background when compared to the case of $\Omega_{R0} = 1$ [Fig. 6 (a), (b)]. At longer evolution times a portion of $\rho_{\uparrow}^{(1)}(x;t)$ can escape to the periphery of the BEC leading to a gradual delocalization of $\rho_{\uparrow}^{(1)}(x;t)$ which later on contracts towards the trap center and conducts afterwards a similar behavior. Due to the impurity migration among the spin states $\rho_{\downarrow}^{(1)}(x;t)$ has a complementary structure to $\rho_{\uparrow}^{(1)}(x;t)$ developing humps in the location of the $\rho_{\uparrow}^{(1)}(x;t)$ dips while remaining within the spatial extension of the medium. The above-effects crucially depend on the timescale of the development of impurity-BEC correlations ($\sim \xi/c$) when compared to the corresponding one set by the trap ($\sim \omega^{-1}$), thus exposing the emergence of the locally adiabatic regime. Moreover, the medium is almost perfectly coherent since $|\bar{g}_B^{(1)}(x, x' \neq x)| \approx 0.95$ [Fig. 7 (d)]. However, the spin- \uparrow impurity experiences more severe coherence losses [Fig. 7 (e)]. Indeed, the impurity portion remaining within the bosonic background is adequately coherent namely $|\bar{g}_{\uparrow}^{(1)}(-1.7 < x < 1.7, -1.7 < x' < 1.7)| \approx 0.8$ while the segments escaping the medium are less coherent within themselves and between each other, see for instance $|\bar{g}_{\uparrow}^{(1)}(2 < x < 7, 2 < x' < 7)| \approx 0.5$. Note also that the impurity portion escaping the medium is almost fully incoherent with the one remaining inside its spatial

extent.

By comparing the time-averaged spectra in [Fig. 4 (d)], we observe that the $V_{eff}(x; g_{BI})$ method is able to predict the location of the polaronic resonances emerging for $\Delta > -26$ while it neglects those resonances appearing for $\Delta < -26$ e.g. at $\Delta_+ \approx -28.4$. Also, $\bar{f}(\Delta)$ obtained using $V_{eff}(x; g_{BI})$ has an overall lower amplitude when compared to the MB case. This is attributed to the incoherent fraction of impurity atoms exhibiting TOC, a process that is not captured within $V_{eff}(x; g_{BI})$, similarly to the $\Omega_{R0} = 1$ case. The resonant peaks building upon $f(\Delta)$ in the MB scenario are present also in the case of two non-interacting bosonic impurities with the ones appearing for $\Delta > -27$ being slightly shifted and those for $\Delta < -26$ having a relatively larger amplitude than for $N_I = 1$. Here, the existence of impurity-impurity induced interactions materializes in a shift of the spectral lines whilst their higher amplitude is most probably caused by the smaller lifetime of the impurity excitations when $N_I = 2$ due to a more pronounced TOC. We note that the multi-peaked structure of $\bar{f}(\Delta)$ witnesses that $\Omega_{R0} = 10$ here is proximal but can not be classified into the diabatic spin-transfer regime since it substantially deviates from a Lorentzian distribution. Recall that this observation is in sharp contrast to the $g_{BI} = 0.5$ scenario [Fig. 2 (e)] as well as to $g_{BI} = -0.5$ that will be shown later on [Fig. 4 (f)] where in both cases $\bar{f}(\Delta)$ at $\Omega_{R0} = 10$ represents a Lorentzian being in good agreement with the outcome of the diabatic approximation. As a consequence, we can deduce that for increasing impurity-medium interaction strength the diabatic spin-transfer regime is entered for larger bare Rabi frequencies. This result is attributed to the prominent role of impurity-phonon correlations developing for $t \approx \xi/c$.

The diabatic spin-transfer regime is indeed realized for increasing Rabi frequency $\Omega_{R0} \gg c/\xi$. A paradigmatic example is provided here e.g. for $\Omega_{R0} = 40$ where as it can be seen in the inset of Fig. 4 (d) $\bar{f}(\Delta)$ within the MB approach has a Lorentzian shape for both $N_I = 1$ and $N_I = 2$ and it coincides with the prediction of the diabatic approximation. Apparently, $V_{eff}(x; g_{BI})$ yields the same outcome, suggesting that MB excitation channels are strongly suppressed. The polaronic resonance in all cases is positioned at $\Delta_+^* \approx -24$.

To illustrate how the spectrum is modified with the pulse intensity, we depict $\bar{f}(\Delta)$ for varying Ω_{R0} in Fig. 5 (b). As expected, a power broadening of $\bar{f}(\Delta)$ takes place for increasing Ω_{R0} leading to a perfectly shaped Lorentzian distribution for $\Omega_{R0} \gg c/\xi$, see the inset of Fig. 5 (b). The latter is a case example of the diabatic spin-transfer regime [inset of Fig. 4 (d)]. In contrast, for small Ω_{R0} , satisfying $\Omega_{R0} \leq c/\xi$, the spectral line $\bar{f}(\Delta)$ has several peaks which correspond to distinct polaronic states. Accordingly, these resonances become narrower and their position is shifted [hardly visible in Fig. 5 (b)] for decreasing Ω_{R0} , e.g. see $\bar{f}(\Delta)$ for $\Omega_{R0} = 0.1$ and $\Omega_{R0} = 10$.

C. Attractive Bose polaron: mode-coupling and signatures of induced interactions

Next we aim to study attractive impurity-medium coupling, e. g. $g_{BI} = -0.5$. The resulting spectral response $f(\Delta; \tau)$ and its time-average $\bar{f}(\Delta)$ for $\Omega_{R0} = \omega = 1 \ll c/\xi$ are provided in Fig. 2 (e) and Fig. 4 (e) respectively. A polaronic resonance located at $\Delta_+^* = 8.8$ appears in the rf signal, characterized by a single Rabi frequency $\Omega_R(\Delta_+^*) \approx 0.99$, see the inset in Fig. 2 (e) where the Fourier spectrum of $f(\Delta; \tau)$ is depicted. This resonance is the energetically lowest interacting state of the spin- \uparrow impurity with the bath and manifests as the formation of an attractive Bose polaron [3, 53]. The dressed Rabi frequency is $\Omega_R(\Delta) = \sqrt{(Z\Omega_{R0})^2 + (\Delta - \Delta_+^*)^2}$ with $Z \approx 0.99$, as identified in the spectrum. The underlying polaron generation mechanism can also be inferred from the impurity spin densities which undergo single frequency Rabi oscillations among each other [Figs. 8 (a), (b)]. Indeed, the periodic revival of density lumps in $\rho_{\uparrow}^{(1)}(x; t)$ inside the medium signals the polaron formation which subsequently causes small amplitude perturbations in $\rho_B^{(1)}(x; t)$ [inset of Fig. 8 (b)] due to weakly excited phononic modes triggered by the back-action of the impurity to its environment, see also Ref. [45].

Additional peaks at smaller detuning in $f(\Delta; \tau)$, refer either to higher-lying polaronic states or to resonant coupling between the impurity motion and the collective excitations of the BEC environment [64]. It is worth mentioning that the non-Lorentzian shape of the quasi-particle resonances is an indication that $\Omega_{R0} = 1$ Rabi frequency does not lead to a diabatic spin-transfer; compare the spectral line for the $N_I = 1$ MB case and the

diabatic approximation shown in Fig. 4 (e).

To explicitly identify the polaronic resonances, we utilize the effective potential model which here for the spin- \uparrow impurity corresponds to a harmonic oscillator of effective frequency $\omega_{eff} = \sqrt{1 + (|g_{BI}|/g_{BB})} \approx \sqrt{2}\omega$ within the Thomas-Fermi approximation [53]. The lowest-lying state have energies $\epsilon_n \approx \hbar\sqrt{2}\omega(n + 1/2)$, where the index n denotes each eigenstate. The respective energy differences are of the order of $\delta\epsilon \approx \sqrt{2} \gtrsim \Omega_{R0} = 1$, meaning that the applied pulse enables the resolution of the individual eigenstates of $V_{eff}(x; g_{BI})$.

Employing the time-averaged spectrum $\bar{f}(\Delta)$ within $V_{eff}(x; g_{BI})$ [Fig. 4 (e)] we indeed verify the existence of the individual polaronic states whose positions are in perfect agreement with those predicted by the MB approach. Particularly, the peaks at $\Delta_+ \approx 6.2$, $\Delta_+ \approx 5.4$ and $\Delta_+ \approx 3.2$ signify motionally excited states of the polaron and display a Rabi frequency $\Omega_R(\Delta)$ which is smaller to the one for $\Delta_+^* = 8.8$ [see the dashed box in the inset of Fig. 2 (e)]. This decreasing behavior of Ω_R is attributed to the reduced overlap of these states, and hence reduced quasi-particle residue, with the initial non-interacting impurity-bath MB state [3]. The motionally excited nature of such states can be readily deduced e.g. from the three-peaked structure of the spin- \uparrow impurity density during the pulse time, see Fig. 8 (e). At such detuning, a slow population transfer from the spin- \downarrow to the spin- \uparrow state and vice versa occurs with the $\rho_{\downarrow}^{(1)}(x; t)$ residing around the trap center [Fig. 8 (e), (f)]. Also, the motion of the spin- \uparrow impurity portion weakly disturbs $\rho_B^{(1)}(x; t)$, which subsequently emits small amplitude sound waves [inset of Fig. 8 (f)].

On the other hand, the spectral peaks e.g. at $\Delta_+ \approx 7.4$ in $\bar{f}(\Delta)$ that are not captured with $V_{eff}(x; g_{BI})$, are resonances for the impurity motion with the collective excitations of the BEC medium [53, 64], see Fig. 4 (e). This mode-coupling can be demonstrated, for instance, by monitoring the underlying densities of the individual components [Figs. 8 (c), (d)]. A particle transfer between the $|\uparrow\rangle$ and the $|\downarrow\rangle$ impurity states is evident, accompanied by a breathing motion of $\rho_{\uparrow}^{(1)}(x; t)$ and $\rho_{\downarrow}^{(1)}(x; t)$ which lie near the trap center. Most importantly, when the population of the polaron $|\uparrow\rangle$ state is dominant, $\rho_B^{(1)}(x; t)$ exhibits an enhanced breathing dynamics due to the impurity back-action [inset of Fig. 8 (d)].

Turning to the spectral response of two non-interacting bosonic impurities in the MB case we observe that the structural configuration of $\bar{f}(\Delta)$ is almost the same to the one for $N_I = 1$, see Fig. 4 (e). This indicates that the majority of the polaronic resonances is of single-particle origin. However, by closely inspecting $\bar{f}(\Delta)$ it becomes evident that the position of some of the emergent peaks referring to polaronic excitations, e.g. located at $\Delta_+ = 5.8$, $\Delta_+ = 4.2$ are shifted towards larger detunings when compared to the $N_I = 1$ scenario by an average amount of $\delta\Delta_+ \approx 0.4$. This latter behavior suggests the

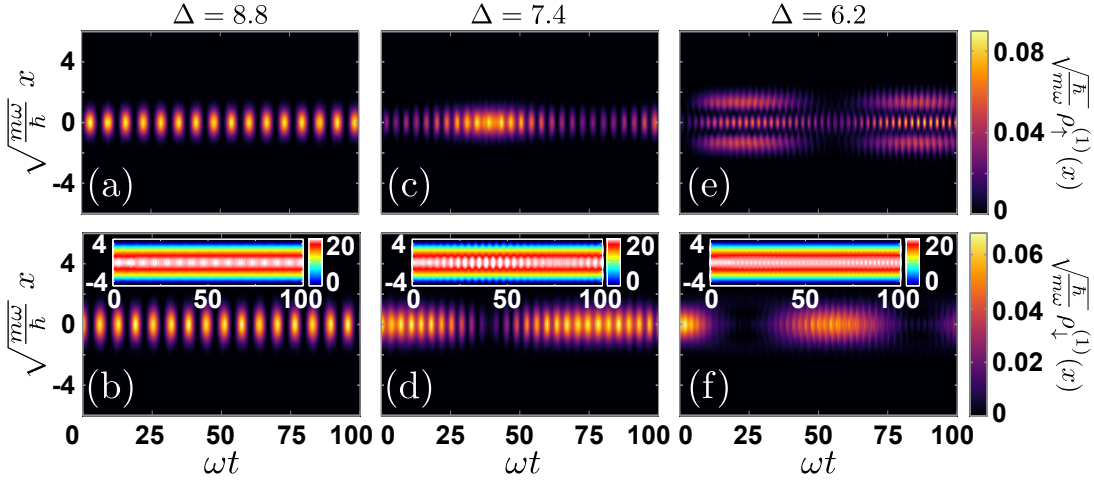


FIG. 8. Spatiotemporal evolution of the density (a), (c), (e) $\rho_{\uparrow}^{(1)}(x;t)$ and (b), (d), (f) $\rho_{\downarrow}^{(1)}(x;t)$ of a single impurity for distinct detunings Δ of the rf field (see legends) and constant bare Rabi frequency $\Omega_{R0} = 1$ visualizing different motionally excited states of the attractive polaron. The insets in (b), (d), (f) show the corresponding density evolution $\rho_B^{(1)}(x;t)$ of the bosonic medium featuring (b), (f) phonon emission and (d) an excited breathing mode. The interaction strengths of the spinor parts of the impurity with the background are $g_{B\downarrow} = 0$ and $g_{B\uparrow} \equiv g_{BI} = -0.5$. Other system parameters are considered to be the same as in Fig. 2. In all cases the employed pulse time refers to $\tau = T = 100 > t$, while the Thomas-Fermi radius of the background is $R_{TF} \approx 4.2$.

appearance of attractive induced impurity-impurity interactions mediated by the bosonic gas [17, 32, 54, 89]. Similar manifestations of induced interactions have been revealed in the spectrum of the contrast of bosonic impurities obtained via the Ramsey response [53]. Let us note is passing that the two-body character of the polaronic resonances will be further discussed in the next section IV.

The rf spectrum for a larger bare Rabi frequency such that $\omega \ll \Omega_{R0} = 10 < c/\xi$ but still $g_{BI} = -0.5$ changes drastically when compared to the $\Omega_{R0} \leq \omega$ scenario. Monitoring $f(\Delta; \tau)$ we observe the appearance of a single polaronic resonance located at $\Delta_+^* \approx 8.8$ which Rabi oscillates in the course of the pulse time [Fig. 2 (f)] while possessing a frequency that obeys $\Omega_R(\Delta) = \sqrt{(Z\Omega_{R0})^2 + (\Delta - \Delta_+^*)^2}$ with $Z \approx 1$ as shown in the inset of Fig. 2 (b). The time-averaged signal $\bar{f}(\Delta)$ is Lorentzian and coincides between $N_I = 1$ and $N_I = 2$. In this sense, two-body processes are here suppressed. Also, the effective potential approximation for $N_I = 1$ provides exactly the same $\bar{f}(\Delta)$ indicating that MB processes are negligible. To exemplify whether the diabatic spin-transfer regime has been realized we compare $\bar{f}(\Delta)$ among the MB method and the diabatic approximation [Fig. 4 (f)]. The two spectra are almost equivalent and thus $\Omega_{R0} = 10 < c/\xi$ essentially acts as a diabatic pulse, a result that stems from the weakly attractive impurity-BEC interactions.

Inspecting $\bar{f}(\Delta)$ for various Ω_{R0} it allows us to infer the adiabatic and the diabatic nature of the employed rf pulse [Fig. 5 (c)]. Indeed, for $\Omega_{R0} \gg \omega$ the time-averaged spectral line as captured by $\bar{f}(\Delta)$ has a Lorentzian form indicating its proximity to the intense pulse case. In ad-

dition, it exhibits a single polaronic peak whose position depends on Ω_{R0} and as a result of the power broadening its width increases for a larger Ω_{R0} . However, in the case of adiabatic spin-transfer ($\Omega_{R0} \leq \omega$) the spectrum is substantially overall narrower and most importantly it shows a multitude of polaronic resonances for $\Delta < \Delta_+^*$ corresponding to energetically higher-lying excitations of these quasi-particles. For instance, as discussed above considering $\Omega_{R0} = 1$ a variety of resonances appear in $\bar{f}(\Delta)$ while for $\Omega_{R0} = 0.1$ only a single narrow peak occurs. The latter observation can be attributed to the fact that the number of the resonant peaks when $\Omega_{R0} \leq \omega$ is of course reduced for smaller Ω_{R0} since then the intensity of the pulse decreases and thus it is less probable to populate higher-lying motionally excited states of the impurity MB spectrum.

IV. CHARACTERISTIC TWO-BODY POLARON PROCESSES: RABI OSCILLATIONS AND CORRELATION INDUCED DEPHASING

To elucidate the existence of possible two-body correlation mechanisms that contribute in the polaron dynamics (in the presence of two impurities) for varying Rabi frequency and detuning of the rf field we invoke the spin-spin probability

$$P_{aa'}(t) = \langle \Psi(t) | \hat{P}_{aa'} | \Psi(t) \rangle. \quad (11)$$

The participating spin operators read $\hat{P}_{\uparrow\uparrow} = |1, 1\rangle \langle 1, 1|$, $\hat{P}_{\downarrow\downarrow} = |1, -1\rangle \langle 1, -1|$ and $\hat{P}_{\uparrow\downarrow} = |1, 0\rangle \langle 1, 0| + |0, 0\rangle \langle 0, 0|$, where the spin basis $|S, S_z\rangle$ is used. These probabilities satisfy $P_{\uparrow\uparrow}(t) + P_{\downarrow\downarrow}(t) + P_{\uparrow\downarrow}(t) = 1$. Apparently,

the limiting cases $P_{\uparrow\uparrow}(t) = 1$ and $P_{\downarrow\downarrow}(t) = 1$ refer to the formation of a two and a single polaron state respectively, whilst $P_{\downarrow\downarrow}(t) = 1$ signifies the absence of polaronic excitations. Below we discuss the behavior of $P_{aa'}(t)$ exemplarily for specific impurity-medium interaction strengths, bare Rabi frequencies (corresponding to adiabatic or diabatic spin-transfer) and different detunings of the rf scheme. Especially by focusing on parameter regions (Ω_{R0}, Δ) where the spectral line peaks between $N_I = 1$ and $N_I = 2$ impurities do not differ we showcase that even in these cases two-body mechanisms play a role for the adequate interpretation of the polaron dynamics.

Regarding attractive impurity-bath couplings namely $g_{BI} = -0.5$ we present $P_{aa'}(t)$ for $\Omega_{R0} = 1$ and $\Delta = 9$ in Fig. 9 (a). Recall that this parameter choice corresponds to the lowest-lying polaron state in $f(\Delta; \tau)$ while the resonance position remains the same for $N_I = 1$ and $N_I = 2$, see also Fig. 2 (e). An almost perfect precession dynamics from the $|\downarrow\downarrow\rangle$ [$P_{\downarrow\downarrow}(t)$] to the $|\uparrow\uparrow\rangle$ [$P_{\uparrow\uparrow}(t)$] spin states and vice versa takes place, a process that gives rise to the periodic formation of a two polaron state. Notice the small reduction of the amplitude of both $P_{\downarrow\downarrow}(t)$ and $P_{\uparrow\uparrow}(t)$ in the course of time which is indicative of a correlation induced dephasing mechanism. Simultaneously, $P_{\uparrow\downarrow}(t)$ oscillates with an almost $\pi/4$ phase difference with respect to both $P_{\downarrow\downarrow}(t)$ and $P_{\uparrow\uparrow}(t)$ but most importantly it exhibits a modulated amplitude, i.e. a beating behavior. The latter observation hints towards the presence of weak impurity-impurity correlations mediated by the bath since in the absence of impurity correlations $P_{\uparrow\downarrow}(t)$ would perform constant amplitude oscillations according to $P_{\uparrow\downarrow}(t) = 2A(t)[1 - A(t)] \sin^2(Z\Omega_{R0}t/2) + (1/2)A^2(t) \sin^2(Z\Omega_{R0}t)$ with $A(t)$ denoting the amplitude of the $f(\Delta; \tau)$ oscillations [70].

Keeping fixed $\Omega_{R0} = 1$ and $g_{BI} = -0.5$ but moving to the spectral peak located at $\Delta_+ = 7.6$ which alludes to the resonance of the impurity motion with the background breathing mode we find that the ensuing dynamics of $P_{aa'}(t)$ is much more complex than for $\Delta = 9 = \Delta_+^*$ [Fig. 9 (b)] and it contains two predominant frequencies. Indeed, the response of $P_{\downarrow\downarrow}(t)$ and $P_{\uparrow\uparrow}(t)$ evinces a slow drift from the $|\downarrow\downarrow\rangle$ to the $|\uparrow\uparrow\rangle$ state with a period $T_1 \approx 55$. The timescale of this process is in line with the one referring to the maximal occupation of $\rho_{\uparrow}^{(1)}(x; t)$, see e.g. Figs. 8 (c), (d) when $N_I = 1$ and note that for $N_I = 2$ the relevant time-interval exhibits a slight shift due to the impurity-impurity effective interactions. The probabilities $P_{aa'}(t)$ exhibit additional faster oscillations having a significantly larger frequency and testifying a population transfer from $P_{\downarrow\downarrow}(t)$ towards $P_{\uparrow\downarrow}(t)$ (single-polaron) and $P_{\uparrow\uparrow}(t)$ (two-polarons). This population transfer occurs due to the resonance at $\Delta_+ = 9$ since $|\Delta - \Delta_+| = 1.4 \sim \Omega_{R0}$ yielding detuned Rabi-oscillations with $\Omega_R \approx 1.72$. Notice that in the time-intervals $0 < t < T_1/3$ and $2T_1/3 < t < T_1$ $P_{\uparrow\downarrow}(t)$ oscillates in-phase [out-of-phase] with $P_{\uparrow\uparrow}(t)$ [$P_{\downarrow\downarrow}(t)$] and vice

versa within $T_1/3 < t < 2T_1/3$. Furthermore, as in the previous case, the oscillation amplitude of $P_{\uparrow\downarrow}(t)$ is not fixed in the time-evolution which suggests once more the existence of weakly attractive induced impurity-impurity interactions mediated by the BEC medium.

Next, we focus on strong impurity-medium interactions i.e. $g_{BI} = 1.5$ where the TOC occurs and study $P_{aa'}(t)$ [Fig. 9 (c)] for an rf pulse possessing $\Omega_{R0} = 1$ and e.g. $\Delta = -27.2$ namely at the region of the spectral resonance identified in $f(\Delta; \tau)$ [Fig. 2 (c)]. We observe that for short evolution times ($t < 10$), i.e. before the TOC occurs, the two bosonic impurities transfer from their spin $|\downarrow\downarrow\rangle$ configuration to a superposition of $|\downarrow\uparrow\rangle$ states. Later on, $10 < t < 30$, the impurities are majorly transferred with a slower rate to the $|\uparrow\uparrow\rangle$ state whose occupation subsequently ($t > 30$) saturates to a finite value when also $|\downarrow\downarrow\rangle$ is almost completely depopulated. Interestingly, the population of the $|\uparrow\downarrow\rangle$ configuration tends to approach a fixed value due to the population of the $|0, 0\rangle$ state while the $|1, 0\rangle$ one does not contribute. This behavior can be explained by a blockade-like mechanism where the transfer of an impurity to the spin- \uparrow state heavily distorts [53, 56] the bosonic background which consequently hinders the transfer of a second impurity to this state until ($t > 10$) the first one escapes from the medium.

Turning to stronger rf pulses, i.e. $\Omega_{R0} = 10$, and again residing close to the corresponding resonance where $\Delta_+ \approx -26$ [Fig. 2 (d)] the underlying spin-transfer processes are more involved [Fig. 9 (d)]. It becomes apparent that for $t < 4$ a precession spin dynamics occurs where $P_{\downarrow\downarrow}(t)$ and $P_{\uparrow\uparrow}(t)$ oscillate out-of-phase with a non-constant amplitude. The latter indicates that the two-polaron state [see also Fig. 6 (e)] whose occupation is given by $P_{\uparrow\uparrow}(t)$ possesses a different energy from the single-polaron configuration [see $P_{\uparrow\downarrow}(t)$], which in turn suggests the presence of induced impurity-impurity interactions. For later times a portion of the spin- \uparrow impurities [see also Fig. 6 (e)] escapes from the BEC environment resulting in a positive shift of the time-averaged population of the polaron states containing one and two spin- \uparrow atoms. In the same time-interval $P_{\downarrow\downarrow}(t)$ and $P_{\uparrow\downarrow}(t)$ oscillate in-phase and out-of-phase with $P_{\uparrow\uparrow}(t)$. This behavior demonstrates the transfer of the trapped (within the BEC) atoms among their spin states and in particular between the $|1, 0\rangle$ and the $|1, 1\rangle$ ones.

To further expose the presence of impurity-impurity correlations we utilize the spin correlation measure

$$C_{\uparrow\downarrow}(\Delta; t) = 4P_{\uparrow\uparrow}(t)P_{\downarrow\downarrow}(t) - P_{\uparrow\downarrow}^2(t), \quad (12)$$

which takes values in the interval $[-1, 1]$. In particular, if $C_{\uparrow\downarrow}(t) = 0$ evinces the absence of correlations between the spin states of the impurities while for $C_{\uparrow\downarrow}(\Delta; t) > 0$ [$C_{\uparrow\downarrow}(\Delta; t) < 0$] signifies the bunching [anti-bunching] tendency of the impurities in the $|\uparrow\rangle$ and $|\downarrow\rangle$ states or equivalently in the $S_z = \pm 1$ spin configurations. The time-evolution of $C_{\uparrow\downarrow}(\Delta; t)$ for $g_{BI} = -0.5$ and $g_{BI} = 1.5$ with varying detuning is presented in Figs. 9 (e) and (f) respectively. Focusing on $g_{BI} = -0.5$ [Fig. 9 (e)] it be-

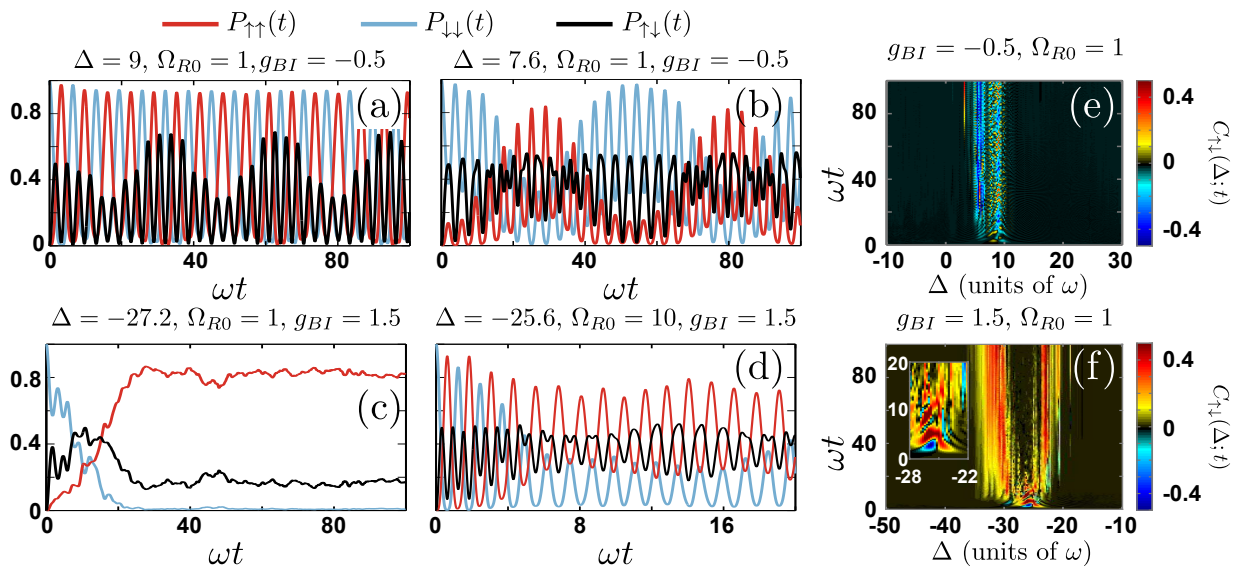


FIG. 9. (a)-(d) Dynamics of the two-body probability [Eq. (11)] for the two non-interacting bosonic impurities to reside both in the spin- \uparrow or the spin- \downarrow state or one in the spin- \uparrow and the other in their spin- \downarrow state for selective detunings and bare Rabi frequencies of the rf field as well as impurity-medium interaction strengths (see legends). The non-constant amplitude of $P_{\uparrow\downarrow}(t)$ signals the development of polaron-polaron induced correlations. Time-evolution of the spin correlator [Eq. (12)] for (e) $g_{BI} = -0.5$, (f) $g_{BI} = 1.5$ with respect to the detuning Δ of the rf field characterizing the correlated spin dynamics of the impurities. The inset of (f) shows the short-time dynamics of the corresponding spin correlator. The two impurities are non-interacting and the bath is composed of $N_B = 100$ bosons with $g_{BB} = 0.5$. The multicomponent setting is mass-balanced, $m_B = m_I$, and it is confined in a harmonic trap of frequency $\omega = 1$. The pulse time in (a), (b), (c), (e), (f) $\tau = T = 100 > t$ while in (d) $\tau = T = 20 > t$.

comes apparent that in the vicinity of the attractive polaron resonance ($7.4 < \Delta < 10.4$), see also Fig. 2 (e), $C_{\uparrow\downarrow}(\Delta; t)$ features an almost periodic behavior exhibiting bunching and anti-bunching of the impurities in the spin- \uparrow and \downarrow states. This process suggests the presence of impurity-impurity induced interactions. Turning to the motionally excited states of the polaron located at $5.2 < \Delta < 6.4$ the correlator $C_{\uparrow\downarrow}(\Delta; t)$ shows a fluctuating character remaining predominantly positive in the course of time thus indicating the two-body nature of these resonances.

For strongly repulsive impurity-medium couplings where the TOC phenomenon takes place the response of $C_{\uparrow\downarrow}(\Delta; t)$ [Fig. 9 (f)] is more involved compared to the attractive interaction case. Indeed, close to the resonance at $\Delta_+^* \approx 26$ an anti-bunching is observed at the initial stages of the dynamics ($t < 5$), as depicted in the inset of Fig. 9 (f), which is another manifestation of the blockade-like mechanism outlined previously, see also Fig. 9 (c). As time-evolves $C_{\uparrow\downarrow}(\Delta; t) > 0$ due to the escape of the spin- \uparrow impurity from the BEC background which allows for the excitation of the second one initially residing in the spin- \downarrow state as also captured by $P_{\uparrow\downarrow}(t)$ [Fig. 9 (c)]. For longer times, $t > 20$, $C_{\uparrow\downarrow}(\Delta; t) \rightarrow 0$ as a result of the population trapping to the spin- \uparrow state due to the TOC. Regarding the lower-lying resonances at $\Delta > -26$ this blockade-like phenomenon is also evident since $C_{\uparrow\downarrow}(t) < 0$ at the initial time-interval of the impurities spin dynamics, see e.g. $13 < t < 30$ for $\Delta_+ = -22.4$. Afterwards the impurities

are bunched in the $|\uparrow\rangle$ state due to the TOC. In contrast, for $\Delta < -30$ the impurities experience a bunching tendency throughout the evolution.

V. HEAVY IMPURITY: BOSE POLARON AND ASSOCIATED INTERFERENCE PROCESSES

Having analyzed in detail the spectral response of an impurity immersed in a BEC environment in the equal mass case, subsequently we intend to unravel the rf spectrum of a heavy impurity and contrast it with the results obtained for the mass-balanced case. To this end, we consider the experimentally relevant mixture of a single ^{174}Yb impurity e.g. residing in the hyperfine states $|F = 2, m_F = 2\rangle$ and $|F = 2, m_F = 1\rangle$ and being immersed in a ^7Li bosonic bath at $|F = 1, m_F = 0\rangle$ while the components are trapped in the same harmonic trap [90]. For convenience we initially focus on repulsive impurity-bath interactions particularly $g_{BI} = 0.5$ and inspect the rf signal for different bare Rabi frequencies, see Figs. 10 (a)-(f).

Regarding $\Omega_{R0} = 1 \ll c/\xi$ we observe a central polaronic peak at $\Delta_+^* \approx -8.8$ in $f(\Delta; \tau)$ showing a dominant Rabi frequency dictated by the relation $\Omega_R(\Delta) = \sqrt{(Z\Omega_{R0})^2 + (\Delta - \Delta_+^*)^2}$ with $Z \approx 0.98$ as displayed in the inset of Fig. 10 (a). Interestingly, a series of additional resonances appear in the spectrum $\tilde{f}(\Delta)$ manifested as peaks for smaller detunings e.g. at $\Delta_+ \approx -10$,

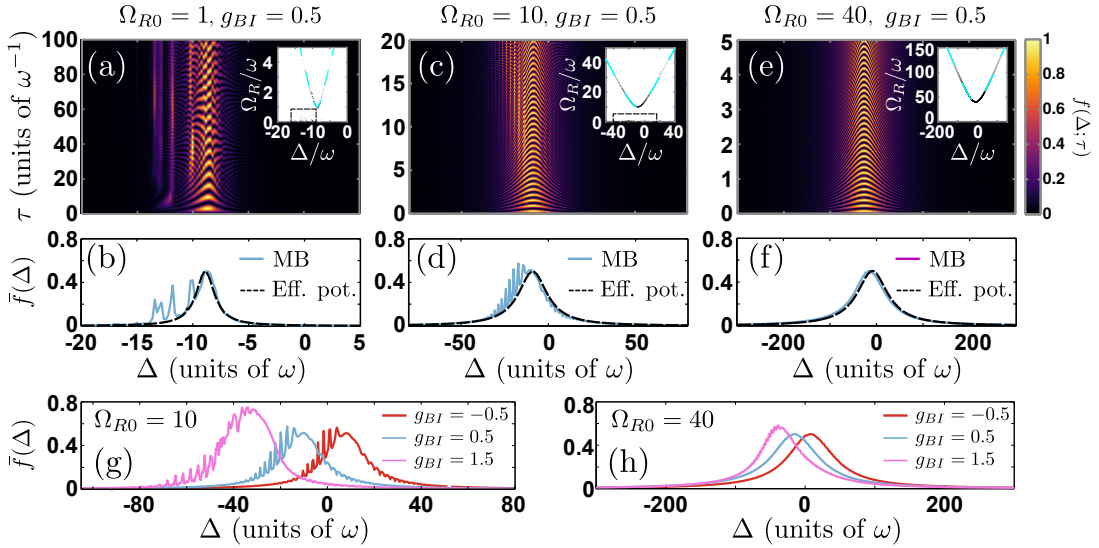


FIG. 10. Time-evolution of the spectroscopic signal $f(\Delta; \tau)$ of a heavy single impurity $N_I = 1$ for varying detuning Δ of the rf field and repulsive impurity-bath interactions $g_{BI} = 0.5$ using a bare Rabi frequency (a) $\Omega_{R0} = 1$, (c) $\Omega_{R0} = 10$ and (e) $\Omega_{R0} = 40$ quantifying the crossover between the distinct spin-transfer regimes. A side peak structure manifests in $f(\Delta; \tau)$ due to the mode-coupling between the polarons and collective excitations of the bath (see text). Insets showcase the spectrum $f(\Delta; \Omega_R)$ whilst the dashed lines provide $\Omega_R(\Delta) = \sqrt{(Z\Omega_{R0})^2 + (\Delta - \Delta_+^*)^2}$ with $\Delta_+^* \approx -8.8$ referring to the position of the resonance and $Z \approx 0.98$ being the quasi-particle residue. Dashed boxes indicate the resolved frequencies Ω_R of the spectral peaks at $\Delta < \Delta_+^*$. Time-averaged spectroscopic signal $\bar{f}(\Delta)$ within the MB method and the effective potential approximation (see legends) for (b) $\Omega_{R0} = 1$, (d) $\Omega_{R0} = 10$ and (f) $\Omega_{R0} = 40$. $\bar{f}(\Delta)$ obtained in the MB approach for different impurity-medium interaction strengths (see legend) for (g) $\Omega_{R0} = 10$ and (h) $\Omega_{R0} = 40$. The system is mass-imbalanced, i.e. $m_I = (174/7)m_B$, and confined in a harmonic trap of $\omega = 1$. It consists of $N_B = 100$ bosons with $g_{BB} = 0.5$ and a single spinor impurity with $g_{B\downarrow} = 0$ and $g_{B\uparrow} \equiv g_{BI}$ indicated in the respective legends.

$\Delta_+ \approx -12$, $\Delta_+ \approx -13.5$ and shallow depletions for a larger Δ located for instance at $\Delta_+ \approx -6.2$, $\Delta_+ \approx -5.8$ and $\Delta_+ \approx -4.2$. Their Rabi frequency [see the dashed box in the inset of Fig. 10 (a)] is appreciably smaller compared to the one for $\Delta_+^* \approx -8.8$ since these motionally excited polaron states have a suppressed overlap with the initial non-interacting state or equivalently decreased residue. As we shall argue below these resonant peaks and depressions refer to the coupling of the impurity motion with the collective excitations, here the breathing mode, of its background. Of course, the effective potential approximation is not able to identify such mode-couplings since by construction it assumes that no medium excitations are induced. For this reason $\bar{f}(\Delta)$ within $V_{eff}(x; g_{BI})$ has a Lorentzian-like form with a single polaron resonance at $\Delta_+^* \approx -8.8$.

The above-described composition of the spectral response remains robust and its features are amplified for a larger bare Rabi frequency, e.g. $\omega \ll \Omega_{R0} = 10 < c/\xi$ illustrated in Figs. 10 (c), (d). Indeed, an overall similar shape of both $f(\Delta; \tau)$ and $\bar{f}(\Delta)$ to the $\Omega_{R0} = 1$ scenario is evident. Namely, there is a polaronic peak located at $\Delta_+^* \approx -10.3$ and side resonances manifested as peaks for $\Delta < \Delta_+^*$ [e.g. at $\Delta_+ \approx -17.1$, $\Delta_+ \approx -20$, $\Delta_+ \approx -22.3$] and depressions of $\bar{f}(\Delta)$ for $\Delta > \Delta_+^*$ [e.g. at $\Delta_+ \approx -0.4$, $\Delta_+ \approx 1.6$, $\Delta_+ \approx 4$]. Notice here that the frequency participating in the underlying spin-flip dy-

namics at Δ_+^* is $\Omega_R(\Delta) = \sqrt{(Z\Omega_{R0})^2 + (\Delta - \Delta_+^*)^2}$, with $Z \approx 0.98$, see the inset of Fig. 10 (c). As explained previously $V_{eff}(x; g_{BI})$ ignores the excitations of the bath and thus can not predict the side peaks of $\bar{f}(\Delta)$ present in the MB case. These side peaks and depressions of the spectrum arise also for a range of impurity-medium interaction strengths while their number is larger for more repulsive couplings as shown in Fig. 10 (g). Also, we can readily infer that the position of the main polaronic resonance depends crucially on g_{BI} .

The origin of this structure of the rf spectrum can be understood as follows. For fixed bare Rabi frequency Ω_{R0} the frequency Ω_R referring to the transfer of the impurity from its spin- \downarrow to the spin- \uparrow state increases as the detuning is shifted away from the polaronic resonance since $\Omega_R(\Delta) = \sqrt{(Z\Omega_{R0})^2 + (\Delta - \Delta_+^*)^2}$ where $Z \approx 0.98$. As a consequence of this periodic transfer, the background density experiences a temporally varying force due to the finite g_{BI} with an “effective” frequency $\sim \Omega_R$. Due to this perturbative force phononic excitations in the form of sound waves are induced in the medium [86] for particular values of Ω_R and therefore for specific Δ . Accordingly, these phononic excitations affect the impurity leading to its modified dressing with respect to the $\Delta = \Delta_+^*$ case signifying enhanced or suppressed polaron formation. This modification in the dressing of the impurity results in a modulation of the rf signal being manifested

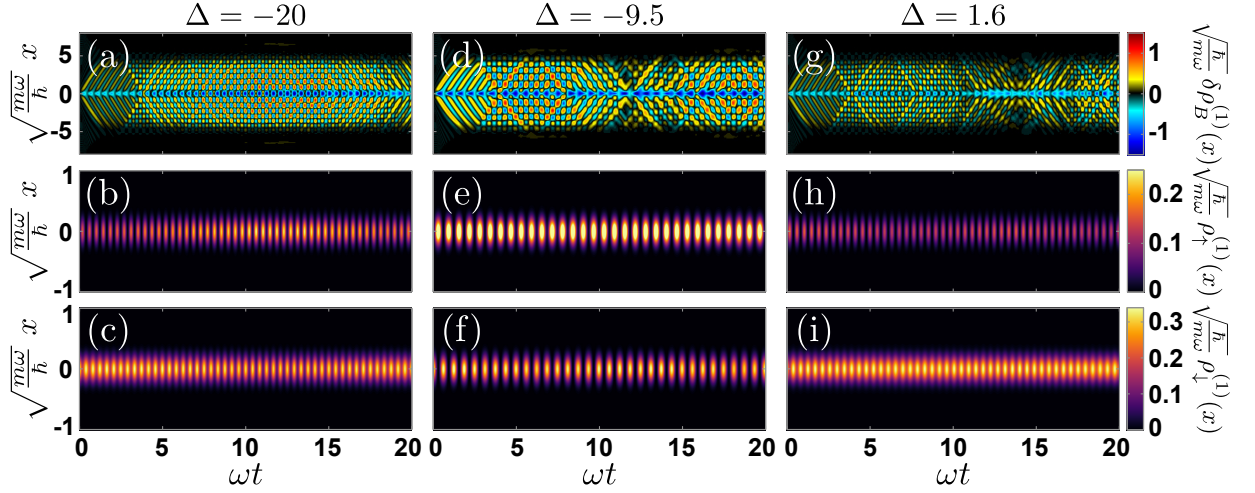


FIG. 11. (a), (d), (g) Temporal fluctuations of the one-body density of the BEC background $\delta\rho_B^{(1)}(x; t) = \rho_B^{(1)}(x; t) - \rho_B^{(1)}(x; 0)$ for different detunings (see legends) and fixed bare Rabi frequency $\Omega_{R0} = 10$. Density evolution (b), (e), (h) $\rho_{\downarrow}^{(1)}(x; t)$ and (c), (f), (i) $\rho_{\uparrow}^{(1)}(x; t)$ of a heavy single impurity for varying Δ (see legends) and constant $\Omega_{R0} = 10$ undergoing Rabi-oscillations. Prominent interference phenomena between the impurity motion and the phononic excitations of the bath are clearly imprinted in $\delta\rho_B^{(1)}(x; t)$. In all cases, $m_I = (133/87)m_B$, $g_{B\downarrow} = 0$, $g_{B\uparrow} \equiv g_{BI} = 0.5$ are considered and the remaining parameters are the same as in Fig. 10. In all cases the pulse time corresponds to $\tau = T = 100 > t$ and the Thomas-Fermi radius of the bosonic bath is $R_{TF} \approx 4.2$.

in the spectrum as an almost equidistant series of side peaks for $\Delta < \Delta_+^*$ and local depressions for $\Delta > \Delta_+^*$.

To corroborate our above argumentation we showcase the density evolution of the spin states and the bosonic bath for specific detunings, corresponding to a peak ($\Delta_+ \approx -20$), the main resonance ($\Delta_+^* \approx -9.5$) and a depression ($\Delta_+ \approx 1.6$) of the $\bar{f}(\Delta)$ with $\Omega_{R0} = 10$ and $g_{BI} = 0.5$. More precisely, for the BEC medium we monitor its density fluctuations i.e. $\delta\rho_B^{(1)}(x; t) = \rho_B^{(1)}(x; t) - \rho_B^{(1)}(x; 0)$, see also Eq. (9), in order to subtract its initial (ground state) background with $\rho^{(1)}(0, 0) \approx 16$ and render the emission of the phononic excitations of amplitude ~ 1 visible. Monitoring $\rho_{\uparrow}^{(1)}(x; t)$ and $\rho_{\downarrow}^{(1)}(x; t)$ we observe that independently of the detuning a Rabi-oscillation, i.e. a periodic population transfer from the $|\uparrow\rangle$ to the $|\downarrow\rangle$ state, takes place [see Figs. 11 (b), (c), (e), (f), (h), (i)] with a frequency according to $\Omega_R(\Delta) = \sqrt{(Z\Omega_{R0})^2 + (\Delta - \Delta_+^*)^2}$ where $Z \approx 0.98$. This process signifies the periodic polaron generation in the system. Most importantly the bosonic bath experiences a more involved dynamical response which is crucially affected by the value of the detuning [Figs. 11 (a), (d), (g)]. The spin- \uparrow impurity motion imprints a prominent sound wave emission for $t < 4$ as it can be seen in $\delta\rho_B^{(1)}(x; t)$ [85, 86] since here $\Omega_R(\Delta) \sim \Omega_{R0} \sim c/\xi$ with the latter referring to the characteristic phonon energy scale. Therefore, the corresponding side resonance structure of $\bar{f}(\Delta)$ [Fig. 10 (d)] is accordingly attributed to the locally adiabatic character of the spin-transfer. In particular, these sound waves emanating from the trap center travel towards its edges and are reflected back. Subsequently, a detuning

dependent interference pattern occurs within the spatial extent of the bosonic bath. Indeed, for detunings corresponding to a side peak (depletion) of $\bar{f}(\Delta)$ the sound waves interfere constructively around $x = 0$ yielding pronounced oscillations of the bath density around the trap center, see Figs. 11 (a) and (g) respectively. These density oscillations in turn periodically modulate the resonant frequency since $\Delta_+^* \propto g_{BI}\rho_B^{(1)}(0; t)$, resulting in an enhanced (reduced) polaron formation for $\Delta > \Delta_+^*$ ($\Delta < \Delta_+^*$), see also remark in Ref. [91].

Further increasing the bare Rabi frequency of the rf field such that $\Omega_{R0} \gg c/\xi$ and operating with $g_{BI} = 0.5$ practically leads to the diabatic spin-transfer regime. This fact is explicitly demonstrated in $f(\Delta; \tau)$ and $\bar{f}(\Delta)$ upon applying a pulse of $\Omega_{R0} = 40$ [Fig. 10 (c)]. It becomes evident that $f(\Delta; \tau)$ features a polaronic resonance at $\Delta_+^* \approx -15.2$ and Rabi oscillates with a frequency of $\Omega_R = \sqrt{(Z\Omega_{R0})^2 + (\Delta - \Delta_+^*)^2}$ and $Z \approx 0.98$, see the inset of Fig. 10 (c). Since in this case the mode-coupling resonances (i.e. the side-peaks) are smeared out, the effective potential approximation can sufficiently predict the resultant rf spectrum $\bar{f}(\Delta)$ [Fig. 10 (f)] because impurity-BEC correlations hardly develop within the small timescale that the impurity resides in the spin- \uparrow state. Similar conclusions, in this strongly driven regime, can also be drawn for the spectral configuration when considering different impurity-medium couplings, see Fig. 10 (h). For instance, the form of $\bar{f}(\Delta)$ remains the same when $g_{BI} = \pm 0.5$ with the resonance being shifted to positive detunings if $g_{BI} = -0.5$. Interestingly, for large impurity-bath repulsions e.g. $g_{BI} = 1.5$ additional side peaks and depressions build upon the spectral

line $\bar{f}(\Delta)$, a phenomenon that is reminiscent of the previously discussed weak pulse scenario. Especially, the peaks originate from the presence of strong interactions leading to the build-up of enhanced impurity-bath correlations.

VI. SUMMARY AND OUTLOOK

We have emulated reverse rf spectroscopy of one-dimensional and harmonically trapped Bose polarons at different spin-transfer regimes ranging from the adiabatic to the diabatic limit as quantified by the intensity of the applied rf field. In this sense, we expose the alterations of the impurity spectral response stemming from fully adiabatic and diabatic rf pulses providing also insights into the intriguing intermediate spin-transfer regime termed as locally adiabatic. This investigation enables us to discern the emergent correlation induced mechanisms of the underlying spin-flip dynamics from single-particle ones and to analyze the origin of the formation of polaronic excitations or mode-couplings of the latter with collective excitations of the background. The location of the identified polaronic resonances depends on the impurity-bath coupling for fixed bare Rabi frequency of the rf field and vice versa. The analysis is based on a variational non-perturbative treatment of the impurities nonequilibrium dynamics that allows us to capture the interparticle correlations of the multicomponent setup. Comparisons with an effective potential approach and the diabatic approximation are performed yielding further insights into the nature of the observed spectral resonances.

Focusing on weakly attractive or repulsive impurity-medium interactions we exemplify the formation of coherent attractive or repulsive Bose polarons respectively. In particular, for pulses characterized by a bare Rabi frequency smaller or equal to the trap one we identify a multitude of polaronic resonances in the spectrum referring to lower and motionally excited states of the generated quasi-particle as well as couplings of the impurity motion with the excitations (breathing mode) of the bosonic bath. These excited states are associated, for instance, with a multihump shape of the impurity density and the emission of sound waves in the bosonic environment. In the case of repulsive interactions the involved spin-mixing dynamics contains a variety of frequencies while for attractive couplings it only involves a single one. An effective potential picture is also constructed to interpret the nature of the polaron excitation processes which are inherently related to a decreasing quasi-particle residue for increasing polaron energy. Considering two bosonic impurities the existence of induced interactions for attracting impurity-medium couplings can be inferred from the small shift of specific spectral resonances. Increasing the bare Rabi frequency such that it exceeds the one set by the energy scale of phononic excitations, the transition to the diabatic spin-transfer regime is verified with the spectrum exhibiting a single polaronic resonance and

its shape being adequately predicted by the diabatic approximation.

Turning to strongly repulsive impurity-bath coupling strengths and for weak bare Rabi frequencies we probe the dynamical decay of the Bose polaron, termed TOC and manifested by the prominent saturation trend of the rf signal for long pulse times. The resultant spectral response features a variety of resonances evincing the existence of distinct superpositions of energetically lower-lying polaronic excitations. The latter can be intuitively understood in terms of an effective potential approximation which accurately predicts the locations of the corresponding spectral peaks. Inspecting the spatiotemporal evolution of the spin densities we observe the build up of their multihump shape supporting the excitation process of the impurity. Remarkably, the decay of the Bose polaron is associated with an energy transfer from the impurity to the BEC background and a suppressed coherence of the former, with both processes being enhanced for a weaker pulses. In the case of two impurities slight shifts in the position of specific spectral peaks with respect to the ones of a single impurity are indicative of the presence of induced impurity-impurity interactions. To further demonstrate the importance of induced interactions we unravel a blockade-like phenomenon by studying the populations of one and two polaron states. Utilizing a larger bare Rabi frequency of the rf field which overcomes the characteristic one of phononic excitations we can systematically reach the diabatic spin-transfer regime represented by a Lorentzian distribution and featuring a single polaronic resonance. Interestingly, the range of Rabi frequencies which can yield a multi-peaked spectral response is broader here when compared to weaker interactions owing to the emergence of the locally adiabatic regime.

The spectrum of an impurity heavier than the atoms of its bath is drastically modified when compared to the equal mass scenario. Here, the spectral response possesses a complex structure independently of the impurity-medium coupling and the bare Rabi frequency of the rf field such that we do not enter the diabatic regime. It consists of a polaronic resonance accompanied by a series of equidistant side peaks and depletions. These side resonances signify the coupling of the impurity spin dynamics with the sound wave excitations of the background yielding pronounced interference phenomena which are especially prominent in the locally adiabatic spin-transfer regime. Naturally, they can not be captured with an effective potential approximation, which does not account for the excitations of the bath, while their number is larger for increasingly repulsive interactions. For sufficiently large Rabi frequencies we reach the diabatic spin-transfer regime where the side peaks and depressions are smeared out and the spectral response has a Lorentzian shape showing a single polaronic resonance in perfect agreement with the diabatic approximation.

There is a plethora of interesting extensions of the present results that are worth being pursued in the fu-

ture. Certainly, the generalization of the current findings to higher spatial dimensions and to the case of both Bose and Fermi impurities exposing this way also the role of the different statistics is extremely desirable. Moreover, it is important to study the robustness of the emergent spin-flip dynamics in the current and higher-dimensional settings in the presence of temperature effects [58, 60, 92, 93]. Another intriguing direction would be to unravel the rf spectrum at different spin-transfer regimes of magnetic quasi-particles such as magnetic polarons or Bose polarons embedded in a spinor bosonic medium. Here, also the investigation of the properties of the rf dressed quasi-particles, e.g. their lifetime, residue, effective mass and induced interactions would be a relevant topic.

Appendix A: Diabatic approximation

As discussed in the main text, Sec. II A, for rf pulses characterized by a bare Rabi frequency $\Omega_{R0} \gg c/\xi$ we enter the *diabatic spin-transfer regime* and impurity-medium correlations are expected to be suppressed since the spatial part of the MB wave function can not adapt to the small timescale of the pulse. Indeed, in this case where $\Omega_{R0} \gg c/\xi$ it is possible to invoke the so-called diabatic approximation for approximating the injection spectrum of the impurities being embedded in the BEC environment. The key assumption of this approximation is that the kinetic energy of both the impurities and the medium is negligible within the duration of the pulse and can therefore be safely dropped. Note that the diabatic approximation does not rely on the omission of the kinetic energy of the system's initial state provided that the corresponding momentum satisfies $\langle p_\sigma(0) \rangle \ll m\Omega_{R0}\xi/\pi$ with $\sigma = B, I$. In fact, for $\Omega_{R0} \gg c/\xi$ the resulting Rabi oscillation of the impurities between their spin- \downarrow and spin- \uparrow states occurs at a much faster timescale i.e. $\sim 1/\Omega_{R0}$ when compared to the relative movement between the bath and the impurity atoms being of the order of $\sim \xi/c$. The latter corresponds to the characteristic timescale where the elementary excitations of the BEC can appear. Accordingly, it is legitimate to treat the atoms as stationary during the injection pulse. The diabatic approximation greatly simplifies the MB Hamiltonian of Eq. (1) whose approximate form reads

$$\begin{aligned} \hat{H}_{\text{diab}} = & \int dx \left\{ \frac{1}{2} m \omega^2 x^2 \left[\hat{\Psi}_B^\dagger(x) \hat{\Psi}_B(x) + \hat{\Psi}_\uparrow^\dagger(x) \hat{\Psi}_\uparrow(x) \right. \right. \\ & \left. \left. + \hat{\Psi}_\downarrow^\dagger(x) \hat{\Psi}_\downarrow(x) \right] + \frac{g_{BB}}{2} \hat{\Psi}_B^\dagger(x) \hat{\Psi}_B^\dagger(x) \right. \\ & \times \hat{\Psi}_B(x) \hat{\Psi}_B(x) + g_{BI} \hat{\Psi}_B^\dagger(x) \hat{\Psi}_\uparrow^\dagger(x) \\ & \left. \times \hat{\Psi}_\uparrow(x) \hat{\Psi}_B(x) \right\} + \frac{\hbar \Delta}{2} \hat{S}_x + \frac{\hbar \Omega_{R0}}{2} \hat{S}_y. \end{aligned} \quad (\text{A1})$$

Here, the parameters ω , g_{BB} , g_{BI} , Δ and Ω_{R0} denote the trapping frequency, individual interparticle interactions,

detuning and bare Rabi frequency respectively and are essentially the same as the ones appearing in Eq. (1). Importantly, notice that since the interparticle interaction is zero-range, \hat{H}_{diab} is diagonal in real space. A crucial corollary of the above fact is that within \hat{H}_{diab} the state of the bath cannot change during the time-evolution. Turning to the impurities, their spatial distribution as captured by their total density, $\rho_I^{(1)}(x) = \rho_\uparrow^{(1)}(x) + \rho_\downarrow^{(1)}(x)$, remains constant in the course of the dynamics. Nevertheless, the spatial distribution of their spin- \uparrow and spin- \downarrow components is allowed to evolve due to the finite Ω_{R0} . To further simplify our analysis we assume here that similarly to the situation described in the main text the bath and the impurity are initially non-interacting, since $\langle \Psi(0) | \hat{S}_z | \Psi(0) \rangle = -1$. Hence, the impurity-medium entanglement is initially zero. This implies that the state of the bath and the impurities possesses the product form $|\Psi(0)\rangle = |\Psi_B(0)\rangle \otimes |\Psi_I(0)\rangle$. As a consequence \hat{H}_{diab} can be projected to the subspace where the bath remains in its initial state, yielding the following Hamiltonian for the impurity degree-of-freedom

$$\begin{aligned} \hat{P}_B \hat{H}_{\text{diab}} \hat{P}_B = & E_0 + \frac{\hbar \Omega_{R0}}{2} \hat{S}_x \\ & + \int dx \frac{\hbar}{2} \left(\Delta + \frac{g_{BI} \rho_B^{(1)}(x)}{2} \right) \hat{S}_z(x), \end{aligned} \quad (\text{A2})$$

where $\hat{P}_B = |\Psi_B(0)\rangle \langle \Psi_B(0)|$ is the corresponding projection operator into the bath initial state and $\rho_B^{(1)}(x)$ refers to the one-body density of the bosonic environment. The term E_0 refers to a constant energy shift which, of course, does not contribute to the dynamics and reads

$$\begin{aligned} E_0 = & \frac{1}{2} m \omega^2 \int dx x^2 \left(\rho_B^{(1)}(x) + \rho_I^{(1)}(x) \right) \\ & + \frac{g_{BB}}{2} \int dx \rho_B^{(2)}(x, x). \end{aligned} \quad (\text{A3})$$

In this expression, $\rho_I^{(1)}(x) = \rho_\uparrow^{(1)}(x) + \rho_\downarrow^{(1)}(x)$ is the impurities one-body density and $\rho_B^{(2)}(x, y)$ designates the two-body density of the bath atoms. The projected Hamiltonian, Eq. (A2), can be interpreted as an ensemble of continuously many spin-1/2 particles that are non-interacting among themselves. This ensemble is subjected to a homogeneous Rabi coupling of amplitude Ω_{R0} that possesses a spatially dependent detuning, namely $\Delta(x) = \Delta + g_{BI} \rho_B^{(1)}(x)/2$. Therefore, the time-evolution of the system according to the approximate Hamiltonian Eq. (A1) can be expressed in terms of the solution of a Rabi-coupled two level system [70]. Indeed, the probability to find a spin- \uparrow impurity at position x after a

rectangular pulse of duration t is

$$P_{\uparrow}(x, t; \Delta) = \frac{1}{N_I} \frac{\Omega_{R0}^2 \rho_I^{(1)}(x)}{\Omega_{R0}^2 + \left(\Delta + \frac{g_{BI} \rho_B^{(1)}(x)}{2} \right)^2} \times \sin^2 \left[\sqrt{\Omega_{R0}^2 + \left(\Delta + \frac{g_{BI} \rho_B^{(1)}(x)}{2} \right)^2} \frac{t}{2} \right]. \quad (\text{A4})$$

Furthermore, the rf signal can be evaluated by the integration of the above-mentioned probability in space, i.e. $f(\Delta, \tau) = \int dx P_{\uparrow}(x, t; \Delta)$ and depends only on the one-body densities of the bath ($\rho_B^{(1)}(x)$) and impurity ($\rho_I^{(1)}(x)$) atoms.

Particularly, for the system prepared in its ground state with $g_{BB} > 0$ and $\langle \Psi(0) | \hat{S}_z | \Psi(0) \rangle = -1$ as examined herein, the BEC density is well-described by the Thomas-Fermi profile $\rho_B^{(1)}(x) = \frac{m\omega^2}{2g_{BB}} (R_{TF}^2 - x^2)$, where $R_{TF} = \left(\frac{3g_{BB} N_B}{2m\omega^2} \right)^{\frac{1}{3}}$ refers to the Thomas-Fermi radius. On the other hand, the impurity density possesses a Gaussian form i.e. $\rho_I^{(1)}(x) = \frac{N_I}{\sqrt{\pi}\alpha} e^{-\frac{x^2}{\alpha^2}}$, with $\alpha = \sqrt{\hbar/(m\omega)}$ being the length of the external confinement. In this case, the averaged rf signal is composed of two parts namely, $\bar{f}(\Delta) = \bar{f}_1(\Delta) + \bar{f}_2(\Delta)$. The first term corresponds to the contribution of the impurity density within the spatial region occupied by the BEC and refers to the integral

$$\bar{f}_1(\Delta) = \frac{1}{2\sqrt{\pi}} \int_{-R_{TF}/\alpha}^{R_{TF}/\alpha} dy e^{-y^2} \frac{\tilde{\Omega}^2}{\tilde{\Omega}^2 + (y^2 - \tilde{\Delta})^2}. \quad (\text{A5})$$

Here, $\tilde{\Omega}(\Omega_{R0}) = \frac{2g_{BB}\Omega_{R0}}{g_{BI}\omega}$ and $\tilde{\Delta}(\Delta) = \frac{2g_{BB}}{g_{BI}} \left[\frac{\Delta}{\omega} + \frac{1}{2} \frac{g_{BI}}{g_{BB}} \left(\frac{R_{TF}}{\alpha} \right)^2 \right]$. In addition, the second term corresponds to a Lorentzian shaped peak at $\Delta = 0$, namely

$$\bar{f}_2(\Delta) = \frac{1}{2} \left[1 - \text{erf} \left(\frac{R_{TF}}{\alpha} \right) \right] \frac{\Omega_{R0}^2}{\Omega_{R0}^2 + \Delta^2}, \quad (\text{A6})$$

with $\text{erf}(x)$ being the error function. This term essentially accounts for the impurities lying beyond the

Thomas-Fermi radius of their medium. Typically the BEC is rather extended, i.e. $R_{TF} > \alpha$, resulting to the contribution of $\bar{f}_2(\Delta)$ being rather small. More specifically, for $N_B = 100$, $g_{BB} = 0.5$ employed in Sec. II A, $R_{TF} \approx 4.2$ and accordingly the amplitude of this Lorentzian peak is negligible $f_2(\Delta) < 1.4 \times 10^{-9}$. Regarding the portion of the impurities lying within the BEC, notice that in the regime of the diabatic approximation ($\Omega_R \gg c/\xi$) $\tilde{\Omega} \gg 1$ holds allowing for the calculation of the integral Eq. (A5) which by employing a Taylor expansion yields

$$\bar{f}_1(\Delta) = \frac{1}{2} \frac{\tilde{\Omega}^2}{\tilde{\Omega}^2 + \tilde{\Delta}^2} \left[1 + \frac{\tilde{\Delta}}{\tilde{\Omega}^2 + \tilde{\Delta}^2} + \frac{3}{8} \frac{3\tilde{\Delta}^2 - \tilde{\Omega}^2}{(\tilde{\Omega}^2 + \tilde{\Delta}^2)^2} + \mathcal{O} \left(\frac{\tilde{\Delta}^3}{(\tilde{\Omega}^2 + \tilde{\Delta}^2)^3}, \frac{\tilde{\Omega}^3}{(\tilde{\Omega}^2 + \tilde{\Delta}^2)^3} \right) \right]. \quad (\text{A7})$$

Eq. (A7) dictates that within the diabatic regime an almost perfectly Lorentzian peak is expected to be centered around $\tilde{\Delta}_0 \approx -0.5$, or equivalently $\Delta_0 \approx -\frac{\omega}{2} \frac{g_{BI}}{g_{BB}} \left[\left(\frac{R_{TF}}{\alpha} \right)^2 - \frac{1}{2} \right]$, with half width at half maximum given by $\gamma \approx \Omega_{R0}$. Notice the linear dependence of the width of the peak γ on the applied Rabi frequency Ω_{R0} stemming from the significant power broadening exhibited in the rf spectrum within this regime.

ACKNOWLEDGEMENTS

S. I. M. gratefully acknowledges financial support in the framework of the Lenz-Ising Award of the University of Hamburg. This work is supported by the Cluster of Excellence 'Advanced Imaging of Matter' of the Deutsche Forschungsgemeinschaft (DFG) - EXC 2056 - project ID 390715994. This work has been funded by the Deutsche Forschungsgemeinschaft (DFG, German Research Foundation) - SFB-925 - project 170620586. F. G. acknowledges funding by the Deutsche Forschungsgemeinschaft (DFG, German Research Foundation) under Germany's Excellence Strategy - EXC-2111 - 390814868. H.R.S. acknowledges the support from the NSF through a grant for ITAMP at Harvard University.

[1] L. D. Landau, Phys. Z. Sowjetunion **3**, 644 (1933).

[2] S. I. Pekar, Zh. Eksp. Teor. Fiz. **16**, 335 (1946).

[3] P. Massignan, M. Zaccanti, and G. M. Bruun, Rep. Progr. Phys. **77**, 034401 (2014).

[4] R. Schmidt, M. Knap, D. A. Ivanov, J. S. You, M. Cetina, and E. Demler, Rep. Progr. Phys. **81**, 024401 (2018).

[5] C. Chin, R. Grimm, P. Julienne, and E. Tiesinga, Rev. Mod. Phys. **82**, 1225 (2010).

[6] T. Köhler, K. Góral, and P. S. Julienne, Rev. Mod. Phys. **78**, 1311 (2006).

[7] C. Kohstall, M. Zaccanti, M. Jag, A. Trenkwalder, P. Massignan, G. M. Bruun, F. Schreck, and R. Grimm, Nature **485**, 615 (2012).

[8] M. Koschorreck, D. Pertot, E. Vogt, B. Fröhlich, M. Feld, and M. Köhl, Nature **485**, 619 (2012).

[9] M. Cetina, M. Jag, R.S. Lous, J.T. Walraven, R. Grimm, R.S. Christensen, and G.M. Bruun, Phys. Rev. Lett. **115**, 135302 (2015).

[10] M. Cetina, M. Jag, R. S. Lous, I. Fritsche, J. T. Walraven, R. Grimm, J. Levinsen, M. M. Parish, R. Schmidt, M. Knap, and E. Demler, Science **354**, 96 (2016).

- [11] F. Camargo, R. Schmidt, J.D. Whalen, R. Ding, Jr, G. Woehl S. Yoshida, J. Burgdörfer, F.B. Dunning, H.R. Sadeghpour, E. Demler, and T.C. Killian, *Phys. Rev. Lett.* **120**, 083401 (2018).
- [12] T. Fukuhara, A. Kantian, M. Endres, M. Cheneau, P. Schauss, S. Hild, D. Bellem, U. Schollwöck, T. Giamarchi, C. Gross, I. Bloch, and S. Kuhr, *Nat. Phys.* **9**, 235 (2013).
- [13] J. Catani, G. Barontini, G. Lamporesi, F. Rabatti, G. Thalhammer, F. Minardi, S. Stringari, and M. Inguscio, *Phys. Rev. Lett.* **103**, 140401 (2009).
- [14] N. B. Jørgensen, L. Wacker, K. T. Skalmstang, M. M. Parish, J. Levinsen, R. S. Christensen, G. M. Bruun, and J. J. Arlt, *Phys. Rev. Lett.* **117**, 055302 (2016).
- [15] M.-G. Hu, M. J. Van de Graaff, D. Kedar, J. P. Corson, E. A. Cornell, and D. S. Jin, *Phys. Rev. Lett.* **117**, 055301 (2016).
- [16] Z.Z. Yan, Y. Ni, C. Robens, and M.W. Zwierlein, *Science* **368**, 190-194 (2020).
- [17] F. Scazza, G. Valtolina, P. Massignan, A. Recati, A. Amico, A. Burchianti, C. Fort, M. Inguscio, M. Zaccanti, and G. Roati, *Phys. Rev. Lett.* **118**, 083602 (2017).
- [18] F. Meinert, M. Knap, E. Kirilov, K. Jag-Lauber, M. B. Zvonarev, E. Demler, and H. C. Nägerl, *Science* **356**, 945 (2017).
- [19] J. Catani, G. Lamporesi, D. Naik, M. Gring, M. Inguscio, F. Minardi, A. Kantian, and T. Giamarchi, *Quantum dynamics of impurities in a one-dimensional Bose gas*, *Phys. Rev. A* **85**, 023623 (2012).
- [20] A.N. Wenz, G. Zürn, S. Murmann, I. Brouzos, T. Lompe, and S. Jochim, *Science* **342**, 457-460 (2013).
- [21] F. Grusdt, and E. Demler, *New theoretical approaches to Bose polarons*, *Quantum Matter at Ultralow Temperatures*, 325-411 (2015).
- [22] S. P. Rath, and R. Schmidt, *Phys. Rev. A* **88**, 053632 (2013).
- [23] L. P. Ardila, and Giorgini, *Phys. Rev. A* **92**, 033612 (2015).
- [24] S.I. Mistakidis, G.C. Katsimiga, G.M. Koutentakis, and P. Schmelcher, *New J. Phys.* **21**, 043032 (2019).
- [25] S. I. Mistakidis, G. C. Katsimiga, G. M. Koutentakis, T. Busch, and P. Schmelcher, *Phys. Rev. Lett.* **122**, 183001 (2019).
- [26] S.I. Mistakidis, A.G. Volosniev, N.T. Zinner, and P. Schmelcher, *Phys. Rev. A* **100**, 013619 (2019).
- [27] L. P. Ardila, N. B. Jørgensen, T. Pohl, S. Giorgini, G. M. Bruun, and J. J. Arlt, *Phys. Rev. A* **99**, 063607 (2019).
- [28] F. Grusdt, R. Schmidt, Y. E. Shchadilova, and E. Demler, *Phys. Rev. A* **96**, 013607 (2017).
- [29] F. Grusdt, K. Seetharam, Y. Shchadilova, and E. Demler, *Phys. Rev. A* **97**, 033612 (2018).
- [30] F. Grusdt, G. E. Astrakharchik, and E. Demler, *New J. Phys.* **19**, 103035 (2017).
- [31] J. Jager, R. Barnett, M. Will, and M. Fleischhauer, *Phys. Rev. Research* **2**, 033142 (2020).
- [32] A. S. Dehkharghani, A. G. Volosniev, and N. T. Zinner, *Phys. Rev. Lett.* **121**, 080405 (2018).
- [33] A. Camacho-Guardian, L. P. Ardila, T. Pohl, and G. M. Bruun, *Phys. Rev. Lett.* **121**, 013401 (2018).
- [34] Y. Nishida, *Phys. Rev. Lett.* **114**, 115302 (2015).
- [35] S. I. Mistakidis, L. Hilbig, and P. Schmelcher, *Phys. Rev. A* **100**, 023620 (2019).
- [36] N. A. Kamar, A. Kantian, and T. Giamarchi, *Phys. Rev. A* **100**, 023614 (2019).
- [37] D. Boyanovsky, D. Jasnow, X. L. Wu, and R. C. Coalson, *Phys. Rev. A* **100**, 043617 (2019).
- [38] Y. E. Shchadilova, R. Schmidt, F. Grusdt, and E. Demler, *Phys. Rev. Lett.* **117**, 113002 (2016).
- [39] M.G. Skou, T.G. Skov, N.B. Jørgensen, K.K. Nielsen, A. Camacho-Guardian, T. Pohl, G.M. Bruun, and J.J. Arlt, *Nat. Phys.* pp.1-5 (2021).
- [40] E. Burovski, V. Cheianov, O. Gamayun, and O. Lychkovskiy, *Phys. Rev. A* **89**, 041601 (2014).
- [41] O. Lychkovskiy, *Phys. Rev. A* **91**, 040101 (2015).
- [42] O. Gamayun, O. Lychkovskiy, E. Burovski, M. Malcolmson, V. V. Cheianov, and M. B. Zvonarev, *Phys. Rev. Lett.* **120**, 220605 (2018).
- [43] C. J. Mathy, M. B. Zvonarev, and E. Demler, *Nature Phys.* **8**, 881 (2012).
- [44] M. Knap, C. J. Mathy, M. Ganahl, M. B. Zvonarev, and E. Demler, *Phys. Rev. Lett.* **112**, 015302 (2014).
- [45] S. I. Mistakidis, F. Grusdt, G. M. Koutentakis, and P. Schmelcher, *New J. Phys.* **21**, 103026 (2019).
- [46] Z. Cai, L. Wang, X. C. Xie, and Y. Wang, *Phys. Rev. A* **81**, 043602 (2010).
- [47] T. H. Johnson, S. R. Clark, M. Bruderer, and D. Jaksch, *Phys. Rev. A* **84**, 023617 (2011).
- [48] P. Siegl, S. I. Mistakidis, and P. Schmelcher, *Phys. Rev. A* **97**, 053626 (2018).
- [49] F. Theel, K. Keiler, S.I. Mistakidis, and P. Schmelcher, *New J. Phys.* **22**, 023027 (2020).
- [50] A. Bohrdt, F. Grusdt, and M. Knap, *New J. Phys.* **22**, 123023 (2020).
- [51] G. Ji, M. Xu, L.H. Kendrick, C.S. Chiu, J.C. Brüggengjürgen, D. Greif, A. Bohrdt, F. Grusdt, E. Demler, M. Lebrat, and M. Greiner, *arXiv:2006.06672* (2020).
- [52] K. Keiler, S.I. Mistakidis, and P. Schmelcher, *New J. Phys.* **22**, 083003 (2020).
- [53] S.I. Mistakidis, G.M. Koutentakis, G.C. Katsimiga, T. Busch, and P. Schmelcher, *New J. Phys.* **22**, 043007 (2020).
- [54] S.I. Mistakidis, A.G. Volosniev, and P. Schmelcher, *Phys. Rev. Research* **2**, 023154 (2020).
- [55] T. Lausch, A. Widera, and M. Fleischhauer, *Phys. Rev. A* **97**, 023621 (2018).
- [56] S.I. Mistakidis, G.C. Katsimiga, G.M. Koutentakis, T. Busch, and P. Schmelcher, *Phys. Rev. Research* **2**, 033380 (2020).
- [57] S. Gupta, Z. Hadzibabic, M.W. Zwierlein, C.A. Stan, K. Dieckmann, and C.H. Schunck, E. G. M. van Kempen, B.J. Verhaar and W. Ketterle, *Science* **300**, 1723 (2003).
- [58] W.E. Liu, Z.Y. Shi, M.M. Parish, and J. Levinsen, *Phys. Rev. A* **102**, 023304 (2020).
- [59] W.E. Liu, Z.Y. Shi, J. Levinsen, and M.M. Parish, *Phys. Rev. Lett.* **125**, 065301 (2020).
- [60] D. Dzsojtjan, R. Schmidt, and M. Fleischhauer, *Phys. Rev. Lett.* **124**, 223401 (2020).
- [61] L. Cao, V. Bolsinger, S. I. Mistakidis, G. M. Koutentakis, S. Krönke, J. M. Schurer, and P. Schmelcher, *J. Chem. Phys.* **147**, 044106 (2017).
- [62] L. Cao, S. Krönke, O. Vendrell, and P. Schmelcher, *J. Chem. Phys.* **139**, 134103 (2013).
- [63] S. Krönke, L. Cao, O. Vendrell, and P. Schmelcher, *New J. Phys.* **15**, 063018 (2013).
- [64] P.E. Dolgirev, Y.F. Qu, M.B. Zvonarev, T. Shi, and E. Demler, *arXiv:2008.02416* (2020).

- [65] K. Kasamatsu, M. Tsubota, and M. Ueda, *Int. J. Mod. Phys. B* **19**, 1835 (2005).
- [66] M. Egorov, B. Opanchuk, P. Drummond, B. V. Hall, P. Hannaford, and A. I. Sidorov, *Phys. Rev. A* **87**, 053614 (2013).
- [67] A. Álvarez, J. Cuevas, F. R. Romero, C. Hamner, J. J. Chang, P. Engels, P. G. Kevrekidis and D. J. Frantzeskakis, *J. Phys. B: At. Mol. Opt. Phys.* **46**, 065302 (2013).
- [68] G.C. Katsimiga, S.I. Mistakidis, T.M. Bersano, M.K.H. Ome, S.M. Mossman, K. Mukherjee, P. Schmelcher, P. Engels, and P.G. Kevrekidis, *Phys. Rev. A* **102**, 023301 (2020).
- [69] M. Olshanii, *Phys. Rev. Lett.* **81**, 938 (1998).
- [70] M. O. Scully, and M. Suhail Zubairy, "Quantum optics", Cambridge University Press, 648 (1999).
- [71] C. Cohen-Tannoudji, B. Diu, F. Laloe, and B. Dui, *Quantum Mechanics* vol. **2** (2006).
- [72] C.J. Pethick, and H. Smith, *Bose-Einstein condensation in dilute gases*. Cambridge University Press 2002.
- [73] A.U. Lode, C. Lévêque, L.B. Madsen, A.I. Streltsov, and O.E. Alon, *Rev. Mod. Phys.* **92**, 011001 (2020).
- [74] S. I. Mistakidis, G. C. Katsimiga, P. G. Kevrekidis, and P. Schmelcher, *New J. Phys.* **20**, 043052 (2018).
- [75] R. Horodecki, P. Horodecki, M. Horodecki, and K. Horodecki, *Rev. Mod. Phys.* **81**, 865 (2009).
- [76] M. Roncaglia, A. Montorsi, and M. Genovese, *Phys. Rev. A* **90**, 062303 (2014).
- [77] J. Frenkel, *in Wave Mechanics* 1st ed. (Clarendon Press, Oxford, 1934), pp. 423-428.
- [78] P. A. Dirac, *Proc. Camb. Phil. Soc.* **26**, 376, Cambridge University Press (1930).
- [79] G. C. Katsimiga, G. M. Koutentakis, S. I. Mistakidis, P. G. Kevrekidis, and P. Schmelcher, *New J. Phys.* **19**, 073004 (2017).
- [80] J.H.V. Nguyen, M.C. Tsatsos, D. Luo, A.U.J. Lode, G.D. Telles, V.S. Bagnato, and R.G. Hulet, *Phys. Rev. X* **9**, 011052 (2019).
- [81] H. Kiehn, S. I. Mistakidis, G. C. Katsimiga, and P. Schmelcher, *Phys. Rev. A* **100**, 023613 (2019).
- [82] Note that the use of $\rho_B^{(1)}(x)$ is justified in our case since the shape of the bosonic gas is not strongly distorted during the dynamics and it adequately corresponds to a Thomas-Fermi profile.
- [83] K. Sakmann, A. I. Streltsov, O. E. Alon, and L. S. Cederbaum, *Phys. Rev. A* **78**, 023615 (2008).
- [84] I. Bloch, J. Dalibard, and W. Zwerger, *Rev. Mod. Phys.* **80**, 885 (2008).
- [85] K. Mukherjee, S.I. Mistakidis, S. Majumder, and P. Schmelcher, *Phys. Rev. A* **101**, 023615 (2020).
- [86] O.V. Marchukov, A.G. Volosniev, and I. Aviv, *SciPost Phys.* **10** (2021).
- [87] K.K. Nielsen, L.A.P. Ardila, G.M. Bruun, and T. Pohl, *New J. Phys.* **21**, 043014 (2019).
- [88] M. Knap, A. Shashi, Y. Nishida, A. Imambekov, D. A. Abanin, and E. Demler, *Phys. Rev. X* **2**, 041020 (2012).
- [89] C. Mora, and F. Chevy, *Phys. Rev. Lett.* **104**, 230402 (2010).
- [90] F. Schäfer, N. Mizukami, P. Yu, S. Koibuchi, A. Bouscal, and Y. Takahashi, *Phys. Rev. A* **98**, 051602 (2018).
- [91] A similar spectral structure to the one observed in Figs. 10 (d), (f) can be unveiled by the simple two-level model $\hat{H} = -(\hbar/2)[\Delta_+^* - \delta \sin(\omega t)]\hat{S}_z + (\hbar\Omega_{R0}/2)\hat{S}_x$, with $\omega > \Omega_{R0}$ and $\delta \ll \Omega_{R0}$.
- [92] H. Tajima, and S. Uchino, *New J. Phys.* **20**, 073048 (2018).
- [93] H. Tajima, and S. Uchino, *Phys. Rev. A* **99**, 063606 (2019).